

# FUNDAMENTAL LIMITATIONS ON COSMOLOGICAL CLUSTERING SIMULATIONS DUE TO “N-BODIES”

Randall J. Splinter<sup>1,2</sup>, Adrian L. Melott<sup>3</sup>, Sergei F. Shandarin<sup>3</sup>, and Yasushi Suto<sup>4</sup>  
randal@convex.hp.com, melott@kusmos.phsx.ukans.edu, sergei@kusmos.phsx.ukans.edu,  
suto@phys.s.u-tokyo.ac.jp

## ABSTRACT

Fundamental physical considerations and past tests suggest that there may be a problem with discreteness error in N-body methods widely used in cosmological clustering studies. This could cause problems with accuracy when coupled to hydrodynamics codes.

We therefore investigate some of the effects that discreteness and two-body scattering may have on N-body simulations with “realistic” cosmological initial conditions. For the initial power spectrum of the density fluctuations we choose a pure power-law with the form  $P(k) \propto k^{-1}$ . Such a spectrum approximates many candidate cosmological models on scales of order 10–100  $h^{-1}$  Mpc while keeping the simplicity of self-similar evolution.

We use an identical subset of particles from the initial conditions for a  $128^3$  Particle–Mesh (PM) calculation as the initial conditions for a variety of Particle–Particle–Mesh ( $P^3M$ ) and Tree code runs. The force softening length and particle number in the  $P^3M$  and Tree code runs are varied and results are compared with those of the PM run. In particular, we investigate the effect of mass resolution, since most “high resolution” codes only have high resolution in gravitational force, not in mass. We show the evolution of various statistical measures, including the power spectrum  $P(k)$ , two–point correlation function  $\xi(r)$ , mean pairwise velocity and pairwise velocity dispersion, cluster analysis, genus, cross-correlation of density fields, and measure of phase correlations. The phase-insensitive two–point statistics,  $P(k)$  and  $\xi(R)$  have been known for some time to be affected by force resolution. We show that they are also affected by the number of particles when the force resolution is held constant, and differ in different N–body codes with similar parameters and the same initial conditions. Differences in the *phases* of the Fourier coefficients more strongly reflect considerable differences in the positions of individual particles, the positions and density of the clumps they comprise, and the velocity dispersion on small scales. These measures mostly converge at the mean interparticle separation scale for the lowest mass–resolution code. As more particles are added, but the absolute scale of the force resolution is held constant, the  $P^3M$  and the Tree runs agree more and more strongly with each other and with the PM run which had the same initial conditions, suggesting that the time integration is converging. However, they do not particularly

converge to a PM run which continued the power law fluctuations to small scales (which is possible given more particles)—except when this power in the evolved state is destroyed by smoothing on a coarse mesh corresponding to the absence of that initial power. The convergence of the codes suggests high particle density is necessary for correct time evolution, since many different results cannot all be correct. Our results showing the effect of the presence or absence of small-scale initial power suggest that leaving it out is a considerable source of error on scales of the missing wavelengths, which can be resolved by putting in a high particle density.

Since the codes never agree well on scales below the mean comoving interparticle separation, we find little justification to use results on these scales to make quantitative predictions in cosmology. The range of values found for some quantities spans 50%, but others, such as the amount of mass in high density regions, can be off by a factor of three or more.

*Subject headings:* cosmology:miscellaneous–gravitation–hydrodynamics–methods:  
numerical–dark matter

## 1. Introduction

A fundamental approximation underlying cosmological N-body simulations is that the density field of the universe may be represented by a set of  $N$  discrete particles. The Universe is thought to be dominated by some form of dark matter whose mass is small compared to that of galaxies, probably small compared to that of stars. The formation of structure in most scenarios proceeds from a nearly homogeneous mass distribution with small perturbations. The formation of stars, galaxies, clusters, and superclusters is probably a hierarchical process, built on a spectrum of density perturbations in this background of very low mass particles. In this case, the only significant discreteness is that which emerges as the particles begin to cluster. The particles themselves (atoms, axions, neutrinos, or something else) have such a small mass as to be insignificant compared to that of the aggregates being studied in the simulations. Therefore any successful N-body code should approximate the solution to the Poisson–Vlasov equations. This can be coupled to hydrodynamics, to model the baryonic matter that gave rise to the luminous component. In this case, the gravitational force on each simulation particle should be dominated

---

<sup>1</sup>Center for Computational Sciences, 325 McVey Hall, University of Kentucky, Lexington, KY 40506

<sup>2</sup>Current Address: Hewlett–Packard Company, High Performance Computing Division, 20 Perimeter Summit Blvd, MS 1904, Atlanta, GA 30319–1417

<sup>3</sup>Department of Physics and Astronomy, University of Kansas, Lawrence, KS 66045

<sup>4</sup>Department of Physics and RESCEU, University of Tokyo, Tokyo 113, Japan

by the mean field, with insignificant discreteness effects (of which there are many kinds). To trace exactly the evolution of the *discrete* particle distribution may sometimes be in conflict with this approximation. The correct evolution of the density field, sampled by a set of particles, is supposed to be obtained by properly adjusting the parameter  $a$  which effectively softens the gravitational force like  $\propto (r^2 + a^2)^{-1}$ . (There are a variety of details of the shape of the softening of the potential at short ranges; this is only a representative example). If the dark matter is not modeled as collisionless, the dominant gravitational force on the hydrodynamic component will also be incorrect.

The choice of  $a$  is a subtle problem unresolved in practice. If the real universe consists of galaxies, with no internal degrees of freedom, then  $a$  could be simply set to the typical size of galaxies  $\sim 10$  kpc provided that the number density of simulation particles  $\bar{n}_{\text{sim}}$  is comparable to that of galaxies  $\bar{n}_{\text{gal}} \sim 0.01 h^3 \text{Mpc}^{-3}$ . For a cosmological volume  $\sim (1000 h^{-1} \text{Mpc})^3$ , this requires that the total number of particles is of order  $10^7$ , which was impossible a decade ago but is quite feasible with current existing computational resources. This could appropriately simulate a Universe in which galaxy formation was decoupled from large-scale structure, as often assumed in the 1970's and earlier. Our universe does not seem so simple; the prevailing consensus is that our universe is made up of dark matter particles, possibly with masses ranging from  $m_{\text{DM}} = 10^{-5}$  to 30 eV. If this is the case, their number density is  $3 \times 10^{77} (1\text{eV}/m_{\text{DM}}) \Omega_0 h^2 \text{Mpc}^{-3}$ , where  $\Omega_0$  is the cosmological density parameter. Then simulation particles do not correspond to physical objects but rather provide a method to sample the density field of dark matter in a very sparse manner. In this case  $a$  must be chosen so as to suppress the artificial discreteness and two-body collision effects of the simulation. These effects are negligible for cosmological simulations even if the masses of large stars are typical of the particle size. Therefore they *should be* absolutely suppressed. Of course the interaction between galaxies is important, but galaxy formation is now thought to proceed by a process of hierarchical clustering intimately interwoven with large-scale structure formation. When two-body effects between galaxies are included, internal degrees of freedom must be included as well.

This line of thought naturally indicates that  $a$  should be close to the mean simulation particle separation  $\bar{l}_{\text{sim}} \equiv \bar{n}_{\text{sim}}^{-1/3}$  since  $a \ll \bar{l}_{\text{sim}}$  would manifest the undesirable discreteness due to the sparse sampling of the density field. Hereafter we define  $\epsilon = a \bar{n}_{\text{sim}}^{1/3}$  so that  $\epsilon = 1$  corresponds to this choice. While this is consistent with the PM simulation methodology with one or more particles per cell (e.g. Hockney & Eastwood 1988) the choice of  $\epsilon \lesssim 0.1$  which *intends* to achieve higher spatial resolution is nearly universal in P<sup>3</sup>M and Tree code simulations (e.g., Efstathiou et al. 1985; Sugihara et al. 1991). So the question is whether or not the choice  $\epsilon = 1$  is too conservative and whether or not the choice of  $\epsilon \lesssim 0.1$  correctly traces the evolution of the underlying density field of dark matter while retaining higher spatial resolution without suffering from discreteness effects. This question may have a different answer depending on the intended purpose of the simulation. We attempt to answer it for the case of some statistical measures.

The answer to the above question should depend on the specific problem the simulation is

addressing. Efstathiou & Eastwood (1981) studied collisionality (one effect of discreteness) by means of mass segregation in a P<sup>3</sup>M code with  $\epsilon \lesssim 0.1$  and found significant two-body scattering. Peebles et al. (1989) studied this in a PM code and verified that  $\epsilon \sim 1$  was necessary to suppress collisionality. Both these tests used reasonable perturbation spectra but only had one diagnostic of discreteness effects. It is customary in computational physics to use solutions with known characteristics to test codes before applying them to new problems. The shock tube is now often being used in this way for hydrodynamical simulations in cosmology, although no one thinks galaxies formed this way. Melott et al. (1997) presented a clear case against a use of  $\epsilon < 1$  in one dimensional collapse of a plane wave. This study was restricted to a formal test case and the precise effect on realistic cosmological simulations is not clear.

Often it has been argued that most fluid elements in hierarchical clustering contract, justifying the use of smaller  $\epsilon$  Kuhlman et al. (1996) showed that even for regions of relative overdensity  $\delta > 10$  about half the small fluid elements which contract in one or two directions expand in the third.

Another problem has to do with the use of correct initial conditions. Absence of the initial perturbations on scales smaller than the particle Nyquist wavelength but larger than the force resolution scale results in inaccurate modeling of the merger history of clumps. This cannot be compensated by improving the force resolution. The initial power spectrum above the particle Nyquist frequency could in principle have a wide variety of forms. Therefore, expecting the right answer without putting in the correct initial conditions implies that the final stage completely forgets that important piece of information; this can be only approximately true. As a test of this we generated two PM models identical except for the presence or absence of initial perturbations in the range  $16k_f < k < 64k_f$ , where  $k_f$  represents the fundamental wavenumber corresponding to the simulation box size. Comparing the other models to the first one shows the effect of differences in integration of initial conditions, while comparison to the latter includes the effect of the presence of this part of the initial conditions.

The purpose of the present paper is to quantitatively examine the extent to which discreteness effects in simulations with  $\epsilon < 1$  may change various statistical measures in models with a power spectrum not unlike that present in the range of interest of many viable cosmological clustering theories. It may be somewhat surprising that such a fundamental issue has not yet been examined in detail in the past. The proper comparison between PM, P<sup>3</sup>M and Tree codes (we will generically refer to P<sup>3</sup>M and Tree codes as High Force Low Mass Resolution codes, HFLMR, in this paper) over the dynamical range which we will present below has been feasible for almost a decade on supercomputers, and within reach of high-end workstations for about five years.

## 2. Models

We use PM (Hockney & Eastwood 1988; Melott 1981, 1986), AP<sup>3</sup>M (Couchman 1991), and Tree (Suginohara et al. 1991; Suto 1993) codes. The P<sup>3</sup>M code had adaptive smoothing turned off since we wish to compare a standard P<sup>3</sup>M method. The Tree runs use the fixed smoothing length in comoving coordinates, and we set a tolerance parameter  $\theta = 0.2$  which is considerably smaller (and thus more accurate) than conventional choices ( $\theta = 0.5 \sim 0.75$ ).

The initial power spectrum in all cases was  $P(k) \propto k^{-1}$  up to some cutoff, in most cases at the Nyquist frequency  $k = 16k_f$  dictated by the runs with the fewest particles. Realization of the corresponding density field was generated using the Zel'dovich approximation (Zel'dovich 1970) to perturb the particles from their initial lattice (Doroshkevich et al. 1980). All the models are evolved in the Einstein – de Sitter universe ( $\Omega_0 = 1$ ). The comparisons were performed at three different epochs when the nonlinear wavenumber  $k_{\text{nl}}$  becomes  $16k_f$ ,  $8k_f$ , and  $4k_f$ , where  $k_{\text{nl}} = k_{\text{nl}}(A)$  is defined as

$$\sigma^2(k_{\text{nl}}, A) = A^2 \int_0^{k_{\text{nl}}} P(k) d^3k = 1. \quad (1)$$

In the above  $A$  denotes the expansion factor (unity at the initial condition), and these values of  $k_{\text{nl}}$  correspond to the epochs  $A = 22.36$ ,  $42.13$ , and  $92.20$ , respectively. The latest moment we studied corresponds to nonlinearity on the largest scale which does not suffer from finite-volume boundary condition problems (Ryden & Gramman 1991; Kauffmann & Melott 1992). The specific runs we tested and the model parameters are shown in Table 1. We note that PM codes, which have been extensively used in most physical applications with large numbers of particles, are much faster than the other two types. Thus our  $128^3$  PM runs took much less CPU time than even the  $32^3$  Tree or P<sup>3</sup>M runs. The typical limitation on PM runs is memory or disk space, while CPU time is the typical limitation on P<sup>3</sup>M or Tree runs. HFLMR codes usually run with  $\epsilon < 1$ , but we will examine their behavior over a range in  $N$  and  $\epsilon$ , pushing them toward  $\epsilon = 1$  by increasing the number of particles while keeping the absolute scale of force resolution  $a$  constant. So far as we know, this crucial experiment has not been done before with HFLMR codes.

Our primary strategy is therefore to highlight the largely unexplored mass resolution issue by varying the number of particles while keeping  $a$  constant (it is not *exactly* constant because in fact the shape of the short-range softening function is different in all three codes). Within a given code  $a$  will be constant, so we can spot trends. Between codes softening will be of comparable size. In most cases we set  $a = 1$  (in units where the box size is 128) in both the Tree and P<sup>3</sup>M codes, and run PM with a  $128^3$  mesh. It is typical of HFLMR codes to have  $a$  considerably less than  $\bar{l}_{\text{sep}}$ , the mean interparticle separation over the entire simulation box. In most uses of PM codes, the opposite is true (although in gravitational applications it has become customary to have  $a = 1$  or 0.5).

It is important to note that one cannot represent initial power to higher than the Nyquist wavenumber of the particles or the mesh of the FFT used to impose the initial conditions,

whichever is worse (in fact the latter is rarely a problem in cosmology). Therefore most of our runs only have initial power up to  $k_c = 16k_f$ , so that comparisons of only the effects of divergent numerical integration can be done. The  $N = 64^3$  and  $32^3$  initial conditions are taken from a subset of the  $N = 128^3$  PM runs with the power spectrum cut off at this wavenumber. In order to explore the effect of having initial power at higher wavenumbers which is only possible with more particles, we have one PM run with  $k_c = 64k_f$ . We also have two runs with  $a = 0.25$  to put some points along the pure force resolution axis (which has been emphasized in the past by users of HFLMR codes). These “extra” runs have  $32^3$  particles,  $\epsilon = 0.0625$ , implying  $a = 0.25$ .

We now have for the first time a large number of runs using 3 different codes with identical initial conditions, identical force resolution, but varying mass resolution. In particular the number of particles varies widely enough to study the same physical system with values of  $\epsilon$  typical of HFLMR codes as well as to study the same system with a PM code with similar force resolution *and* matching mass resolution ( $\epsilon = 1$ ).

### 3. Visual Impressions

The lowest order discreteness effect is merely sampling. In Figure 1 we show a slice of the density field of our PM simulation with  $k_c = 16k_f$  at  $k_{nl} = 4k_f$  one cell thick. Both pictures show the same configuration; in one case all of the particles in the slice are available and in the other only those from a  $32^3$  subset are used. The discreteness has a major effect on the visual impression, corresponding to the noise effect on high-order statistics. A claim of filamentarity in the sparse picture would certainly be greeted with skepticism. Although percolation analysis can still detect a signal in such datasets (e.g. Melott et al. 1983) it is still very noisy. The change in discreteness in redshift surveys is largely responsible for the shift in attitude toward superclusters from the 1970’s through the 1980’s. Clumps, filaments, and sheets are progressively harder to see through discreteness noise; many present simulations are able to show filaments but have too few particles to allow sheets to be seen.

More seriously, if these two different density fields were coupled to hydrodynamics, with the dark matter driving the gravitational field, the results would be very different. Of course, both distributions have the same two-point correlation function, but many other things are completely different.

Differences between the runs described in Table 1 can be seen in Figures 2 at different stages of evolution. At a given stage particles which lie within a box at the same location are shown. In cases with more particles, only those with the same initial locations as those of the  $32^3$  subset are shown and used in calculating all statistics for comparison presented hereafter.

There is a general resemblance of all plots at the same stage. Since they all have force resolution  $a \lesssim 1$  if this were the only issue we would expect them to be identical down to the scale of one tick mark. They are not. For example, the three P<sup>3</sup>M runs all with  $a = 1$  ( $\epsilon = 1, 0.5, 0.25$

corresponding to  $N = 128^3, 64^3, 32^3$ ) all look different on scales larger than  $a$ . Within this series, as the number of particles is increased they come to resemble the PM run with  $k_c = 16k_f$ , the same initial condition. The same trend is evident in the Tree runs. Another observation one can make is that on a scale of 4 cells (the mean interparticle separation of the sparsest runs) there are very few apparent differences. The PM run with  $k_c = 64k_f$  looks different from the others, including different from the PM run with  $k_c = 16k_f$ . The overall configuration is similar, but there are many small-scale features reproduced by none of the other models. Consider for example the shape and orientation of (all in this run with extra power) the two largest objects in Fig 2; the existence of the second object in Fig 3; the partial bridge in Fig 4. Power on scales above the force resolution but below the mass resolution of HFLMR has made an apparent difference. Again, on scales of the interparticle separation the differences appear to evaporate. Upon smoothing with a Gaussian of length  $\bar{l}_{sep}$  we see considerable convergence to a common answer. The message here about small scales is that one cannot ignore the initial conditions there and expect the result to be unaffected. HFLMR codes are based on the idea that one can shrink  $\epsilon$  arbitrarily to get higher resolution. We see very real differences implying integration errors for even the modest  $\epsilon = 0.25$ . We expect greater differences for smaller  $\epsilon$ . The transfer of power to small scales is strong, but does not make small-scale initial power totally irrelevant. The reader is referred to the center and bottom center images of Figure 7 in Beacom et al. (1991) for another example of the importance of initial power on small scales even when it is deep in the nonlinear regime.

In the following sections we quantify some of the differences with a variety of statistical measures.

## 4. Statistical Comparisons

This section contains the main body of our results. Although we examine a number of measures, this must be considered a preliminary investigation. We wish to stress that similarity or lack thereof in the studies of one characteristic between various runs should not be construed as implying the same thing for some other purpose. The major phase differences we find later make simple extrapolation based on power amplitudes highly questionable.

### 4.1. Power Spectra

We compute our power spectra on a  $128^3$  mesh with CIC cloud assignment of local density. In all cases we only use  $32^3$  of the particles, so that the discreteness contribution is exactly the same. We have not subtracted off the discreteness contribution from the spectra, because it is not Poissonian at early times and subtraction of such would constitute an error. For consistency we also do not subtract it at late times (when it would in any case be quite small).

In Figure 5 we show the spectrum of the initial conditions evaluated on a series of progressively

finer meshes (the vertical offset is a numerical device to make them visible). The lowest line corresponds to the standard choice of showing things up to the particle Nyquist frequency. However, it is common practice at very late times to show the autocorrelation function to very small radii. This seems to be a contradiction. *If* the initial spectra had been shown to the same resolution, they would look like this (our example is from  $32^3$  particles). Our point is that *if* the code has sufficient force resolution to resolve these spikes (which are not random phase), then those *are* the initial conditions. This study then includes both an examination of integration errors as a function of  $\epsilon$  as well as the effect of the absence of this initial power—two independent but practically intertwined effects.

In Figure 6 are plotted all of the power spectra from the  $32^3$  subset of the runs specified in Table 1 at our three output stages. Considering the diversity of types of codes and their operating parameters, the agreement is encouraging. In the final output stage, major differences are only present beyond about half the mesh Nyquist frequency, i.e.,  $k = 32k_f$ . Some expected trends emerge: the codes with the very smallest  $a$  have the highest amplitude at high frequencies for a given code type. PM codes in general have low amplitude at large  $k$ . Other results are unexpected: Tree codes also have systematically lower amplitude than P<sup>3</sup>M codes with the same  $\epsilon$  at large  $k$ . For both Tree and P<sup>3</sup>M codes, for *fixed*  $a$ , as the number of particles increases, the amplitude increases. This was not anticipated. We speculate that a larger number of particles is better able to handle the mode coupling that accompanies nonlinear evolution.

Some support for this idea can be found in the neighborhood of the “kink” around  $k = 16k_f$  in some evolved spectra in Fig 6 (we temporarily ignore the run with additional high- $k$  power). All the other runs which had the same initial conditions fall into two behavior groups here: those with  $32^3$  particles (dotted or longdash-dot lines), and those with more, without regard to code type, mass or force resolution. All runs with  $32^3$  particles overlie one another, and have the lowest amplitude in the region of the kink. Recalling that  $k = 16k_f$  is the Nyquist frequency of the particles, it is entirely reasonable to suppose that this kink is caused by the inability to transfer power to larger wavenumbers limited by the Nyquist Theorem.

This kink is hidden later; no doubt mode coupling from even longer waves coupled with the considerable deformation of the lattice allows this to fill in. But for some codes—those with fewer particles—a crucial step in the evolution was handled incorrectly. The fact that the power spectrum recovers does not mean the evolution is correct (see also Bouchet et. al 1985). But it probably *does* mean one can get the final power spectrum right to fairly high wavenumbers with almost any code. Note that the point of divergence of the spectra in the evolved state is close to the particle Nyquist wavenumber ( $k = 16k_f$ ). It is tempting to conclude that although spectral agreement is good, one can only have full confidence up to this value. Whether this is a general feature or an accident will require further study.

## 4.2. Two-point Correlation Function

For a long time the two-point correlation function  $\xi(R)$  has been a staple of cosmology studies in large-scale structure. See Peebles (1980) for an excellent exposition. Formally, it is the Fourier transform of the power spectrum discussed in the last section, so no new information is present. However, it is packaged differently, and may allow new insights through new presentation.

In Figure 7 we show the evolution of  $\xi(R)$  at our three stages plotted against separation  $R$  in grid cells (based on  $128^3$  as the box size). We show the spikes which exist at early stages of evolution from a lattice; they are normally suppressed in publication comparing with data by only showing late stages.

Note that differences at the latest stage are not too great. However, there is a noticeable effect at the second stage near  $R = 3$ . All the codes with  $32^3$  particles differ from the rest here. We stress that *all* correlations and spectra are computed using CIC weighting (Hockney & Eastwood 1988) from a set of  $32^3$  particles, even when the original contained many more. Thus this is a systematic difference and not an artifact of sampling.

In the final stage, while there is agreement at larger radii, for  $R < 2$  or twice the force resolution scale of most of our runs, things begin to break down severely. Both dotted lines ( $\epsilon = 0.0625$ ) are high, consistent with the traditional HFLMR emphasis on force resolution. However, the P<sup>3</sup>M code with  $128^3$  particles and  $\epsilon = 1$  is also high. We find evidence that both better mass resolution and better force resolution contribute to maintaining the power law to small radii, which provides support for the use of HFLMR codes to get these statistics without good mass resolution. However, we do not know whether or not it is accidental. Strangely, the P<sup>3</sup>M run with  $64^3$  particles and  $\epsilon = 0.5$  has the lowest amplitude at small  $R$ , occupying a kind of minimum. As we do not have a  $128^3$  tree run, we cannot be sure of the position of the minimum there. Still, its run with  $\epsilon = 0.0625$ ,  $a = 0.25$  overlies the P<sup>3</sup>M run. At any rate, the non-monotonic behavior of the P<sup>3</sup>M run and the observed effect of both force and mass resolution separately varied as well as code differences make it difficult to justify the use of  $\xi$  on scales below about  $2a$ . More study of these effects is needed. We have no way of knowing whether our results on force or mass resolution would continue to change beyond the range in  $N$  and  $a$  studied here. Furthermore, without further study we cannot be sure whether the scale of agreement on  $\xi$  is coupled to the force resolution scale, the mass resolution scale, or some complicated combination of the two.

Conclusions on the two-point correlation: (1)  $\xi(R)$  appears to agree to within 15 separations, (3) It appears that HFLMR may reproduce effects of high mass resolution reasonably well, insofar as  $\xi(R)$  is concerned, and (4)  $\xi$  in N-body simulations for  $R \lesssim 2a$  cannot be regarded as totally reliable, since it changes when either  $N$  or  $a$  is varied independently..

### 4.3. Pairwise Velocities

The statistics which have been discussed up to this point are based purely upon the spatial distribution of the mass. To probe any differences in the dynamics we also need to consider the velocity field. To compare the evolved particle velocities we compute the mean pairwise (PW) velocity and the mean pairwise dispersion (Peebles 1980). We compute the mean pairwise velocity using

$$\langle V_{12}(r) \rangle = \frac{1}{N(r)} \sum_i \sum_{j \neq i} \frac{(\vec{v}_i - \vec{v}_j) \cdot (\vec{r}_i - \vec{r}_j)}{|\vec{r}_i - \vec{r}_j|} \quad (2)$$

where the summation is taken over all the pairs with separation  $r$  and  $N(r)$  the number of such pairs. The PW dispersion,  $\sigma_{V_{12}}(r)$ , is similarly defined by

$$\sigma_{V_{12}}(r) = \sqrt{\frac{1}{N(r)} \sum_i \sum_{j \neq i} \left| \frac{(\vec{v}_i - \vec{v}_j) \cdot (\vec{r}_i - \vec{r}_j)}{|\vec{r}_i - \vec{r}_j|} \right|^2}. \quad (3)$$

In Fig 8 we plot the absolute magnitude of the mean PW velocity and the PW dispersion. There are several clear trends. As expected, when  $\epsilon$  decreases both the PW velocity and dispersion increase. This is because the particles can now approach one another more closely and scatter more strongly off from one another. This trend is also explained in terms of the cosmic virial theorem incorporating the finite size effect of particles (Suto & Jing 1997). There is a more interesting and unexpected trend; as the number of particles is increased (keeping the absolute force resolution fixed) the mean PW velocity and PW dispersion tends to increase. While the above trend with  $\epsilon$  might be expected this trend which depends upon the mass resolution is surprising and substantiates our claim that decreasing the force softening length past the mean particle separation can lead to spurious effects.

### 4.4. Density Cross-Correlation

The density cross-correlation

$$K = \frac{\langle \delta_1 \delta_2 \rangle}{\sigma_1 \sigma_2} \quad (4)$$

was introduced by Coles et al. (1993) as a method to help quantify similarity (or lack thereof) in the density distribution between various models, where in our case  $\delta$  is the density contrast on the ( $32^3$  or  $128^3$ ) mesh and  $\sigma$  is its *rms* value. We compute the cross-correlation on two different sized meshes. One with  $32^3$  cells which corresponds to the mass resolution scale of our lowest mass resolution runs and another with  $128^3$  cells which corresponds to the force resolution scale of our fiducial models. This comparison will help quantify whether the variety of models tested here produce similar or different small-scale structure.

In Tables 2, 3, and 4 we show the density cross-correlations at the nonlinear stages  $k_{nl} = 16k_f$ ,  $8k_f$ , and  $4k_f$ . The table entries above the diagonal are evaluated on a  $128^3$  mesh and the values

below the diagonal on a  $32^3$  mesh. In order to assure uniform treatment, all density fields are computed from a set of  $32^3$  particles which had the same initial conditions. Therefore, any differences are due to systematic differences between the configurations in the evolved state. We ignore here the additional differences introduced purely by sampling effects, as in Figure 1. However, we ran tests to insure that densities computed from full ensembles of particles do not give greatly different results.

The cross-correlations on the  $32^3$  mesh are much better than the cross-correlations on the  $128^3$  mesh. Thus, the codes agree rather well at the mean interparticle separation scale of the coarsest mass resolution runs. This coarse-mesh agreement is generally quite high at all stages for all codes with two exceptions: (1) The Tree code runs with  $32^3$  particles and (2) the PM runs with a full range of initial power  $k_c = 64k_f$  evolve values of  $K$  closer to 0.9 than to 1.0. The first may be due to some large-scale differences due to the absence of a grid in the Tree code while PM and P<sup>3</sup>M codes share the same grid-based algorithm in computing long-range force. The PM results indicate that the absence of initial power on small scales can still be detected, even at late times and on larger scales, when those modes have gone deeply nonlinear. These differences, however, are not large. Even the worst agreement on this mesh is better than the best agreement on the fine ( $128^3$ ) mesh corresponding to the force resolution of most of the runs.

The fine-mesh cross-correlations (shown above the diagonal in Tables 2-4) display a number of interesting patterns: (1) Agreement between codes with the same initial conditions,  $N$ , and  $\epsilon$  monotonically worsens, reflecting amplification of differences. (2) This worsening is much more rapid between runs with the same *small*  $\epsilon$ . For example  $\epsilon = 0.0625$  Tree cross P<sup>3</sup>M (same  $\epsilon$ ) evolves from 0.95 to 0.63 while for  $\epsilon = 0.25$  it goes from 0.96 to 0.70. For the  $N = 64^3$  runs with  $\epsilon = 0.5$ , it goes from 0.90 to 0.84. This is strong evidence that integration errors are being much more strongly amplified for small  $\epsilon$ , as suggested by Suisalu & Saar (1995), and by Park (1997). (3) At a given stage, as  $N$  and  $\epsilon$  are increased, runs with the same initial conditions converge to one another. PM, Tree, and P<sup>3</sup>M all agree rather well in this limit. There are also two islands of consistency in Table 4 between the two P<sup>3</sup>M runs with smallest  $\epsilon$  and  $a$  (0.86), and the two Tree runs with smallest  $\epsilon$  and  $a$  (0.87), but this agreement does not extend to agreement between two *different codes* with small  $\epsilon$  and  $a$ . The convergence for large  $N$  and  $\epsilon$  *does* extend to agreement between different codes. (4) The run with  $k_c = 64k_f$  is the best standard of comparison for appropriate initial conditions in cosmology, since most scenarios have power extending to very small scales, not a cutoff. While the comparisons discussed in (1-3) above highlight differences in integration, (4) includes the effect of the presence or absence of small-scale power. It is only possible to put this power in when a very large  $N$  permits it to be sampled by the particles. Time evolution shows that cross-correlation of the full-sampled run with other runs becomes slowly better, as mode coupling brings down power from larger scales; however, it never really achieves a high value with any other run, regardless of the force resolution of that run. In fact, the runs with smallest  $a$  have the *worst* agreement with this full-sampled run, even though the strategy of small  $a$  is to try to follow clustering on small scales. These results combined with those on the

correlation function/power spectrum appear to indicate that this strategy may partly produce the correct amplitudes of Fourier components, but the wrong phases. Thus it may be that only statistics like the correlation function and the power spectrum which contain no phase information show strong agreements between the various models. Since the differences on small scales lie in phase information, we will look at that in the next section.

#### 4.5. Phase Correlations

Many different configurations can have the same two-point correlation function (or equivalently the same power spectrum) but look completely different. This is due to the difference of the phases of the Fourier component of density field which  $\xi(r)$  and  $P(k)$  ignore. Gaussian-random density fields have statistical properties specified only by amplitudes (since random phases have no information), but the properties of non-Gaussian distributions are dependent on phases. The end results of N-body simulations and the distribution of matter in the Universe are both non-Gaussian, although they may have begun from Gaussian perturbations (as our simulation did; see also Sugimotohara & Suto 1991; Lahav et al. 1993).

Testing for phase agreement is another way of checking for agreement between density fields – in this case those produced by the N-body code. Given phase information for complex numbers  $re^{i\theta}$  specified we use  $\theta = \theta_a - \theta_b$  to specify the difference in phase between two coefficients. Our measure of phase agreement is  $\langle \cos \theta \rangle$ , where the averaging is over spherical shells in  $k$ . This measure is 1 for perfect correlation, 0 for uncorrelated distributions, and negative for anti-correlated ones.

Every correlation coefficient in Tables 2-4 now corresponds to a function of  $k$ . In view of the daunting task of trying to display all these functions, we look instead for patterns. Fortunately, strong ones exist. Figure 9 shows all the data for every run cross-correlated with every other run at the same stage. All data points are plotted but not joined; many overlap.

They segregate in three groups (two of which begin to approach one another at the last stage). (1) The top group (solid squares) corresponds to phase correlations among the group with PM,  $k_c = 16k_f$ , the  $128^3$  and  $64^3$  P<sup>3</sup>M runs and the  $64^3$  Tree runs with the same initial conditions. All runs which fit this definition stay in this "high-agreement" group at all stages. This agreement deteriorates with time, albeit slowly. (2) The bottom row (open circles) corresponds to *anything* compared with the PM,  $k_c = 64k_f$  run. Agreement with this worsens, then gets better, as evolution proceeds. (3) All other phase comparisons lie in a third group (x's). This includes comparisons between various HFLMR runs, which worsen with time.

This third group (x's) lies mostly between the other two, but some comparisons are outliers, joining the top or bottom group. This is not consistent over evolution but a few regularities exist: The outliers (x's) that join the high correlation group (squares) include the two  $32^3$  P<sup>3</sup>M runs compared and the two  $32^3$  Tree runs compared. Each of these pairs are strongly correlated but *do*

*not* correlate well with anything else, across code types or with other runs with the same force resolution, but more particles, within a code type. The outlier x’s that join the bottom (circles) group are, without exception, all comparisons involving one  $32^3$  particle run and one with more particles within a given code, or two  $32^3$  runs from different code types.

These natural groupings correspond to those seen in the density cross-correlations in Tables 2–4. Given the close similarity of the power spectrum in many pairs which cross-correlate badly, we conclude that while differences in phases and amplitudes both exist, the phase differences are primarily responsible for the correlation coefficient differences.

Statistical measures that are sensitive to phase information will clearly suffer more from discreteness than those that are not. The HFLMR strategy may produce a good approximation to the power spectrum but not to anything that depends on phases unless the density field is smoothed over the interparticle separation.

#### 4.6. Displacement vs. Density Contrast

For this series of tests we compare comoving displacement,  $|\vec{\Delta}r|$ , between the PM particles and our standard series of HFLMR runs as a function of the density contrast computed using the PM particles. We compute  $|\vec{\Delta}r(\delta)|$  comparing to both PM models ( $k_c = 16k_f$  and  $64k_f$ ) and at three stages of evolution ( $k_{nl} = 16k_f$ ,  $8k_f$ , and  $4k_f$ ).

There are several trends of interest in these plots. First, in agreement with our results from the density cross-correlation tests comparison with the PM  $k_c = 16k_f$  case appears to produce better  $|\vec{\Delta}r|$  than the PM  $k_c = 64k_f$  case. Secondly, the trend of increasing agreement between the PM and HFLMR codes as  $\epsilon$  is increased also appears to hold here as well. Thus, we see that increasing the number of particles present in the HFLMR codes without changing the absolute force resolution causes their time integration to converge more and more toward the PM code result.

The differences that do exist between different codes with the same initial conditions are amplified as the the particles continue to move apart from one another. Thus, comparing the top three panels of Fig 10, Fig 11, and Fig 12, we see that amplification of errors is more rapid for smaller  $\epsilon$ , even when the force resolution  $a$  is held constant. In Figures 13, 14, and 15 the comparison is done against displacements of particles compared with the PM  $k_c = 64k_f$  run. In this case they are uniformly bad. Although the integration errors are greatly reduced by having more particles, the absence of the extra power in the initial conditions prevents the convergence. None of the runs, regardless of its parameters, comes close.

#### 4.7. Cluster Analysis and Genus

In cluster analysis percolation properties are used to examine the properties of connected regions. Criteria of density thresholds or the close approach of particles are used to decide which clumps are connected. This has been used to study the formation of structure in simulations and in redshift surveys. Percolation properties strongly depend on sampling: the more particles in the model the easier percolation. Obviously percolation in the model corresponding to Fig. 1b is easier than in Fig. 1a.

There are less obvious differences in the number and other properties of overdense regions. Fig. 16 shows three statistics calculated for the subsamples with equal number of particles ( $N = 32^3$ ). The left panels show the fraction of mass in the regions having densities above a given density threshold for all models at three stages of evolution. The middle panels show the fraction of volume occupied by these regions and the right panels show the total number of overdense regions as functions of the density threshold. The clumps were identified by using the percolation code described in Yess & Shandarin (1996). We show the high density part of these distributions. The mass fraction runs from about 0.1% to 10% and the number of clusters from 3 to 300 - 1000. There are significant differences between the models. Unfortunately, the patterns are different at every stages therefore it is difficult to describe them. The differences can be seen more clearly when the ratios are plotted. To do so we choose PM( $k_{nl} = 64k_f$ ) as a fiducial model and plot the logarithms of the ratios in Fig. 17. We also extend the range of densities toward lower densities in this figure so the convergence of the models can be seen.

At the stage  $k_{nl} = 16k_f$  all models converge at about  $\rho < 30$ . In the range  $30 < \rho < 100$  the fiducial PM64 model has more clumps and more mass in clumps than any other model, however at the very high densities  $\rho > 100$  it has fewer clumps and less mass in the clumps than any other model. The typical differences are 2 -3 times. One could expect similar errors on small scales when studying the early stages of clustering, such as Lyman- $\alpha$  absorbers or high-redshift galaxy formation.

At the stage  $k_{nl} = 8k_f$  the differences between models are the least of all three stages. All models except the Tree code with  $N = 32^3, a = 1, \epsilon = 0.25$  have more mass in clumps; they are also more numerous and occupy greater volume. The P<sup>3</sup>M model with  $N = 128^3, a = 1$  has the highest values of all statistics and the Tree code with  $N = 32^3, a = 1, \epsilon = 0.25$  has the lowest. The P<sup>3</sup>M and Tree codes with  $\epsilon = 0.0625, a = 0.25$  are significantly lower than P<sup>3</sup>M model with  $N = 128^3, a = 1$ .

This pattern generally persists at the stage  $k_{nl} = 4k_f$ , however the amplitude of the differences is greater. The P<sup>3</sup>M model with  $N = 128^3, a = 1$  is again among the highest but the P<sup>3</sup>M and Tree codes with best force resolution  $\epsilon = 0.0625, a = 0.25$  are now comparable to it. All the models converge at about  $\rho < 100$ . When the densities are computed on the  $32^3$  mesh the differences are considerably smaller but still are noticeable at the  $k_{nl} = 16k_f$  stage Fig. 18. However, they almost vanish at the final stage. This variation of peak density with particle number is completely

consistent with results presented by Craig (1997) on the central density of halos in N-body simulations.

The genus is a measure of the connectivity of structures widely used in cosmology. It is specifically highly sensitive to phase information. All Gaussian distributions have the same distribution of genus as a function of volume fraction, with the amplitude merely being determined by an integral over the power spectrum. We show the genus here computed using the method of Weinberg et. al (1987). The genus plotted for the last stage of the evolution Fig. 19 is essentially in agreement with the other results: there are differences up to 15% between different codes on the scale of the force resolution (right panel) and almost no differences on the scale of the mean particle separation (left panel). In fact with this smoothing the N-body results are shown to reproduce well the quasi-linear prediction for the genus curve. See Matsubara 1994 and Matsubara & Suto 1995 for details.

Cluster analysis has shown that if the clumps were selected using isodensity surfaces calculated on the force resolution scale then different codes would predict very different numbers of clumps, their total volume and the total mass in the clumps. Differences as large as factor of 2 or 3 are typical for the few hundred largest clusters. The vertical scales in Fig. 16 are about 2 -3 times greater than the horizontal scales depending on the statistics and stage. This means that if one reverses the question and asks what is the difference in the density thresholds provided that same number of clumps (or total mass) selected then the difference in densities would be about 30 - 50%. If the densities are computed on the scale of the mean particle separation then all codes agree with each other at stage  $k_{nl} = 4k_f$  with about 20% accuracy in terms of the numbers, volumes and masses at given density thresholds or with accuracy of 5% in terms of density. These differences are based on clustering, not sampling, since we used the same number of particles for each. However, one can get an idea of the size of a possible sampling effect by comparing the results shown here for PM with a fully sampled PM density field using all  $128^3$  particles. The differences in these statistics between sparse and full PM samples are much smaller than between different codes. Due to the non-monotonic nature of the changes we see with evolution, we cannot make any predictions about how various codes and strategies would compare at later stages of evolution.

## 5. Discussion

A number of the statistical results presented here show only moderate differences between the various codes and our choices of  $a$  and  $\bar{l}_{sep}$ . This is particularly true for the two-point statistics,  $P(k)$  and  $\xi(r)$ , which contain no phase information. On the other hand, for  $\langle V_{12}(r) \rangle$  and  $\sigma_{V_{12}}(r)$  the dependence on  $a$  and  $\bar{l}_{sep}$  is weak, while the dependence is strong for the phase correlations, the mass density and number of clumps, as well as the phase correlations and the density cross-correlations. This implies that the distribution of the phases may be the pivotal piece of information that is needed to resolve this issue. Unfortunately, no satisfactory measure of

the distribution of the phases exists.

It is interesting to keep in mind that in plasma physics (e.g., Hockney & Eastwood 1988) and in beam dynamics (Habib 1997) it is widely recognized that  $\bar{l}_{sep} \ll a$  is a requirement to accurately model a collisionless system. This is in strong contradiction to standard practice in cosmological simulations where  $\bar{l}_{sep} \gg a$ . This is a survival in methodology from the original cosmological N–body simulations which assumed to evolve the distribution of galaxies and *not* the dark matter distribution (in fact, they were generally called ”galaxy clustering simulations” at the time). Note that we cannot appeal to which code produces the best agreement with observations to settle our dilemma. On small scales, where we find significant differences, there is an unknown correspondence between mass and light in the Universe. This issue must be settled by first principles, i.e., agreement on which equations are to be solved and the most accurate methods to solve them.

The sources of the observed errors are *not* random but systematic in origin. It is important to stress that there are two numerical issues; (a) Two codes with identical initial conditions and similar  $a$  and  $\bar{l}_{sep}$  should produce similar statistical results for *all* statistical measures of the evolved particle distribution and not just a subset as we have found here. Our results show a convergence in the time integration between various codes as  $a \sim \bar{l}_{sep}$ . Unfortunately it is *not* standard in cosmology (except in about half the PM applications) to use  $a \sim \bar{l}_{sep}$ . (b) The trouble is that the “correct” initial conditions correspond to our case  $k_c = 64k_f$ . Thus, it appears that the HFLMR codes are not able to correctly model the  $k_c = 64k_f$  solution despite the past claims in the literature and will produce solutions which only agree to  $\bar{l}_{sep}$  and not down to the force softening length  $a$ . This, of course, creates a real dilemma when it comes to simulating truly hierarchical structure PM codes are fast, but the number of particles are limited by disk storage requirements. So–called adaptive mesh refinement algorithms will suffer the same fate as the HFLMR methods tested here since they are unable to input the true power spectrum down to arbitrary scales initially. This leaves us with nested–grid PM methods (Villumsen 1988; Anninos, et al 1994; Splinter 1996) as the best surviving option. These methods allow for both high force and mass resolution simultaneously, thus guaranteeing that  $a \sim \bar{l}_{sep}$  is satisfied on the smallest scales and that the true initial power spectrum is input *ab initio*. *Local* adaptive mesh refinement schemes may offer some advantages if the refinement is carefully designed and tested. This may allow some reduction of the integration error we have demonstrated, but cannot be a substitute for inclusion of the proper initial conditions.

ALM and SFS wish to acknowledge the financial support of the NSF–EPSCoR program, NASA grant NAG5-4039, and the National Center for Supercomputing Applications. ALM also wishes to thank David Weinberg for useful discussions as well as for a an unpublished code comparison project which proved useful. RJS wishes to thank the Center for Computational Sciences at the University of Kentucky for financial support, and Salmon Habib for useful discussions. YS thanks RESCEU (Research Center for the Early Universe, University of Tokyo),

KEK (National Laboratory for High Energy Physics, Japan), and the Astronomical Data Analysis Center of the National Astronomical Observatory (where the Treecode simulation were performed) for a generous allocation of computer time.

## REFERENCES

- Anninos, P., Norman, M., & Clarke, D.A. 1994, ApJ, 436, 11
- Beacom, J.F., Dominik, K., Melott, A.L, Perkins, S.P., & Shandarin, S.F. 1991 ApJ 372, 351.
- Bouchet, F.R., Adam, J.C. & Pellat R. 1985 AA 144,413.
- Coles, P., Melott, A.L., & Shandarin, S.F., 1993 MNRAS 260, 765.
- Couchman, H. 1991 ApJ, 368, L23
- Craig, M. 1997 poster presented at "Dynamics and Statistics of Large-Scale Structures in the Universe", University of Kansas.
- Doroshkevich, A.G., Kotok, E., Novikov, I.D., Polyudov, A.N., Shandarin, S.F., & Sigov, Yu.S. 1980 MNRAS 192, 321.
- Eastwood, J.W., Hockney, R.W., & Lawrence, D.N. 1980 Comp.Phys.Comm. 19, 215.
- Efstathiou, G.E., Davis, M., Frenk, C.S. & White, S.D.M. 1985 ApJS, 57, 241
- Efstathiou, G.E., & Eastwood, J.W. 1981 MNRAS 194, 503.
- Habib, S. 1997, private communication
- Hockney, R.W. & Eastwood, J.W. 1988 Computer Simulation Using Particles (New York: McGraw-Hall), p. 454
- Kauffmann, G.A.M., and Melott, A.L. 1992 ApJ 393,415.
- Kuhlman, B., Melott, A.L., & Shandarin, S.F. 1996, ApJ 470, L41.
- Lahav, O., Itoh, M., Inagaki, S., & Suto, Y., 1993, ApJ, 402, 387
- Matsubara, T, 1994, ApJ, 434, L43
- Matsubara, T, & Suto, Y., 1996, ApJ, 460, 51
- Melott, A.L. 1981 Ph.D. Thesis, University of Texas
- Melott, A.L. 1986 Phys Rev Lett, 56, 1992
- Melott, A.L. & Shandarin, S.F. 1993 ApJ, 410, 469
- Melott, A.L., Splinter, R.J., Shandarin, S.F., & Suto, Y. 1997 ApJ, 479, L79
- Park, C.B. 1997 AAS Poster Presentation.
- Peebles, P.J.E., Melott, A.L., Holmes, M.R., Jiang, L.R., 1989 ApJ, 345, 108
- Peebles, P.J.E., 1980, The Large Scale Structure of the Universe, (Princeton: Princeton University Press)
- Ryden, B.S., and Gramann, M. 1991 ApJ 383, L33.
- Splinter, R.J. 1996, MNRAS, 281, 281
- Suginohara, T., Suto, Y., Bouchet, F.R., & Hernquist, L. 1991, ApJS, 75, 631

- Suginohara, T. & Suto, Y., 1991, *ApJ*, 371, 470
- Suisalu, I., & Saar, E. 1995 preprint astro-ph/9511120
- Suto, Y. 1993, *Prog. Theor. Phys.*, 90, 1173
- Suto, Y. & Jing, Y.P. 1997, *ApJS*, 110, in press
- Villumsen, J.V. 1988, *ApJS*, 71, 407
- Weinberg, D.H., Gott, J.R., and Melott, A.L. 1987 *ApJ* 306, 341.
- Yess, C., & Shandarin, S.F. 1996, *ApJ*, 465, 2
- Zel'dovich, Ya. B. 1970, *A&A*, 5, 84

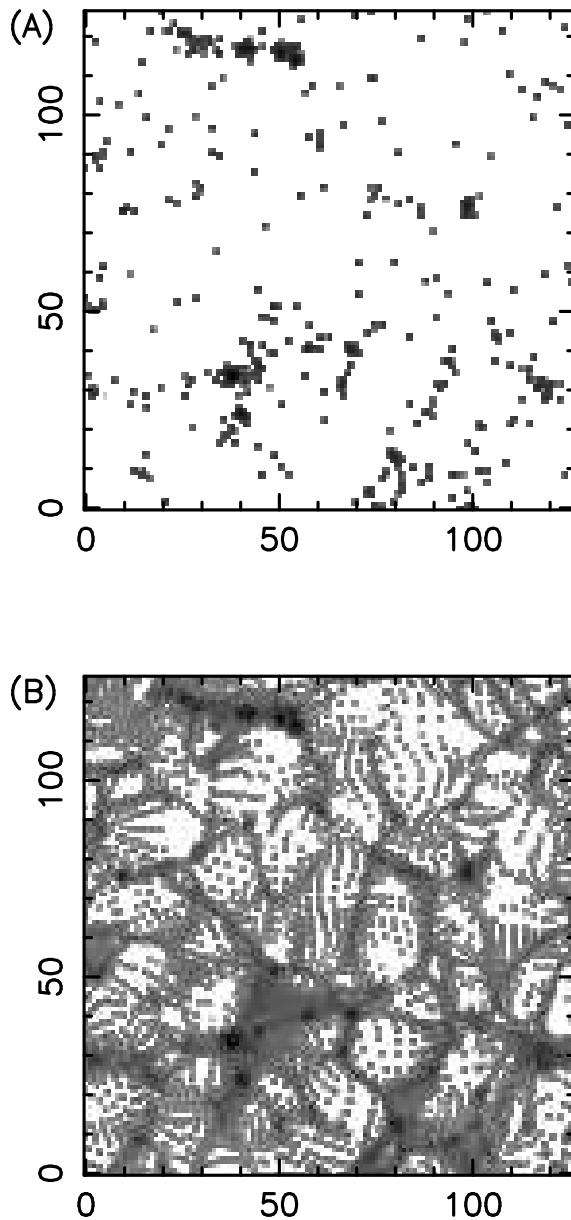


Fig. 1.— We show density fields constructed from a slice of an evolved state of our PM simulation. The parameters of the two images are identical, except that (a) is constructed using only those in the  $32^3$  subset (see text) of particles which happen to lie within the slice. Image (b) is from all of the  $128^3$  particles which lie within the slice. Although the inferred two-point correlation would be identical, the visual impressions are very different, as would be higher-order measures of structure. The general awareness of superclusters which arose in the 80’s is primarily the result of an analogous change in the signal-to-discreteness noise ratio in redshift surveys.

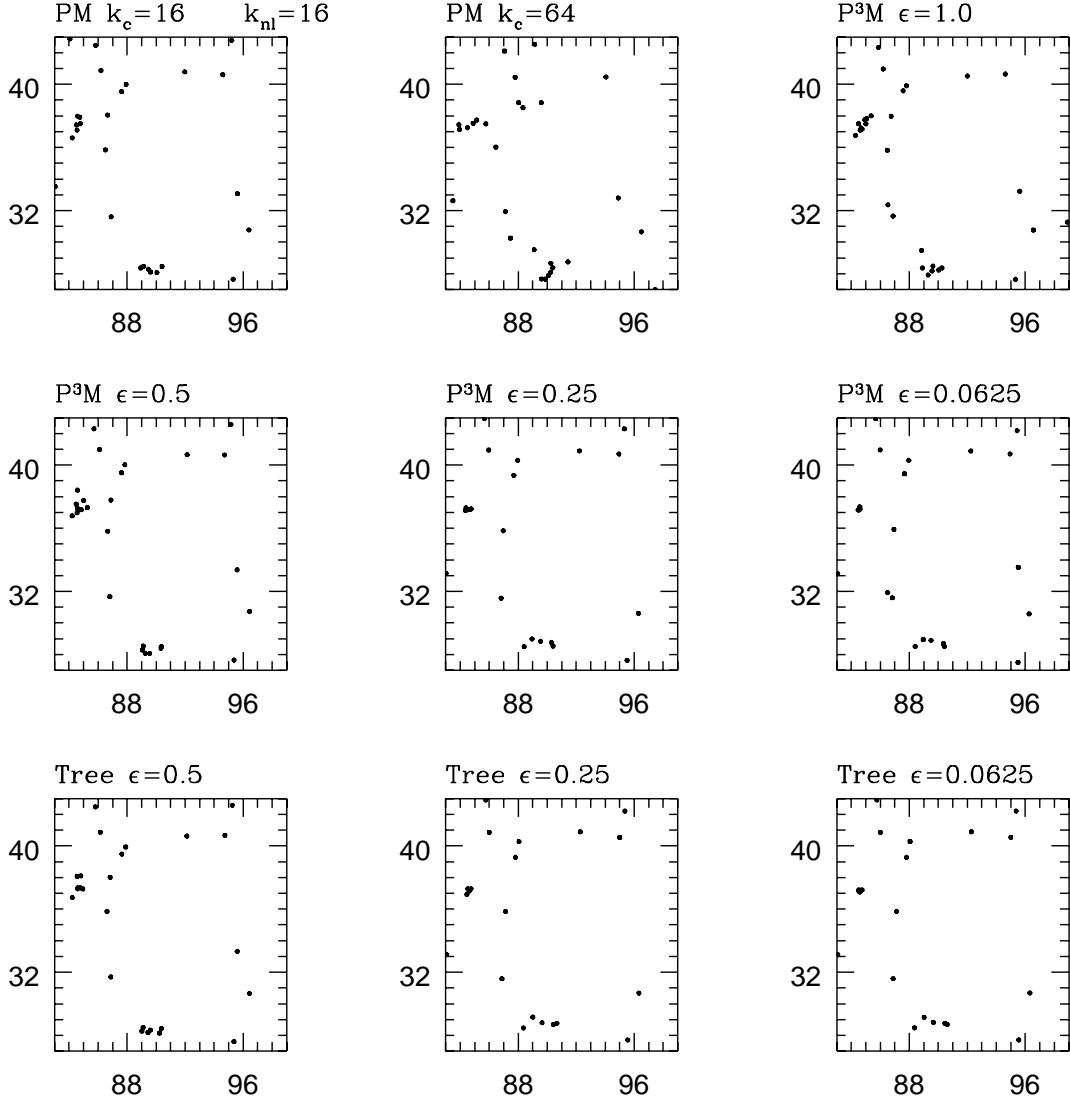


Fig. 2.— For the nine runs listed in Table 1, identified by code type and by  $\epsilon$ , a slice 16 by 16 by 8 cells of a region of average density. Axis units are of the  $128^3$  mesh. For the stage  $k_{nl} = 16k_f$ .

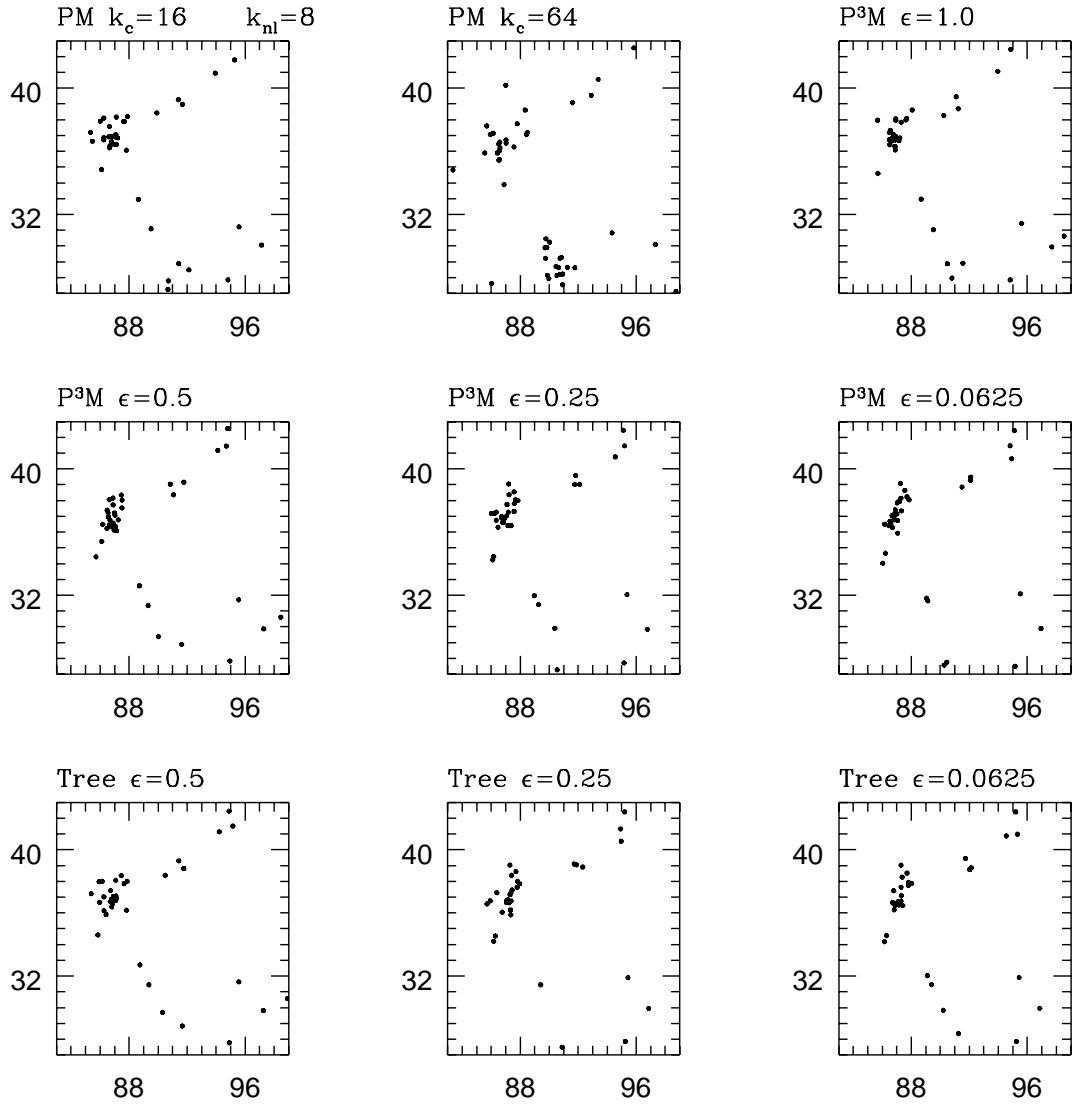


Fig. 3.— As in 2, for the stage  $k_{nl} = 8k_f$ .

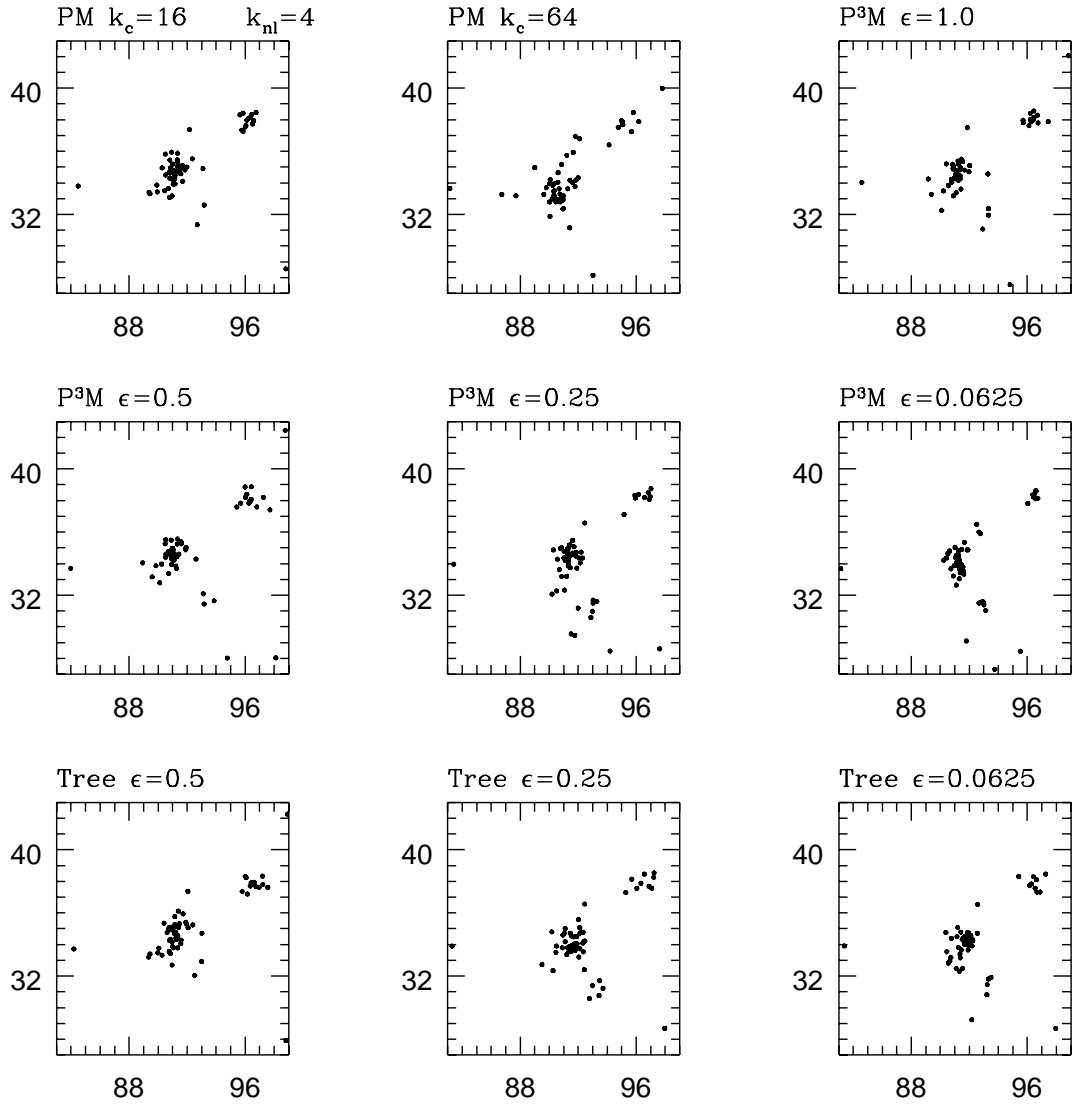


Fig. 4.— As in 2, for the stage  $k_{nl} = 4k_f$ .

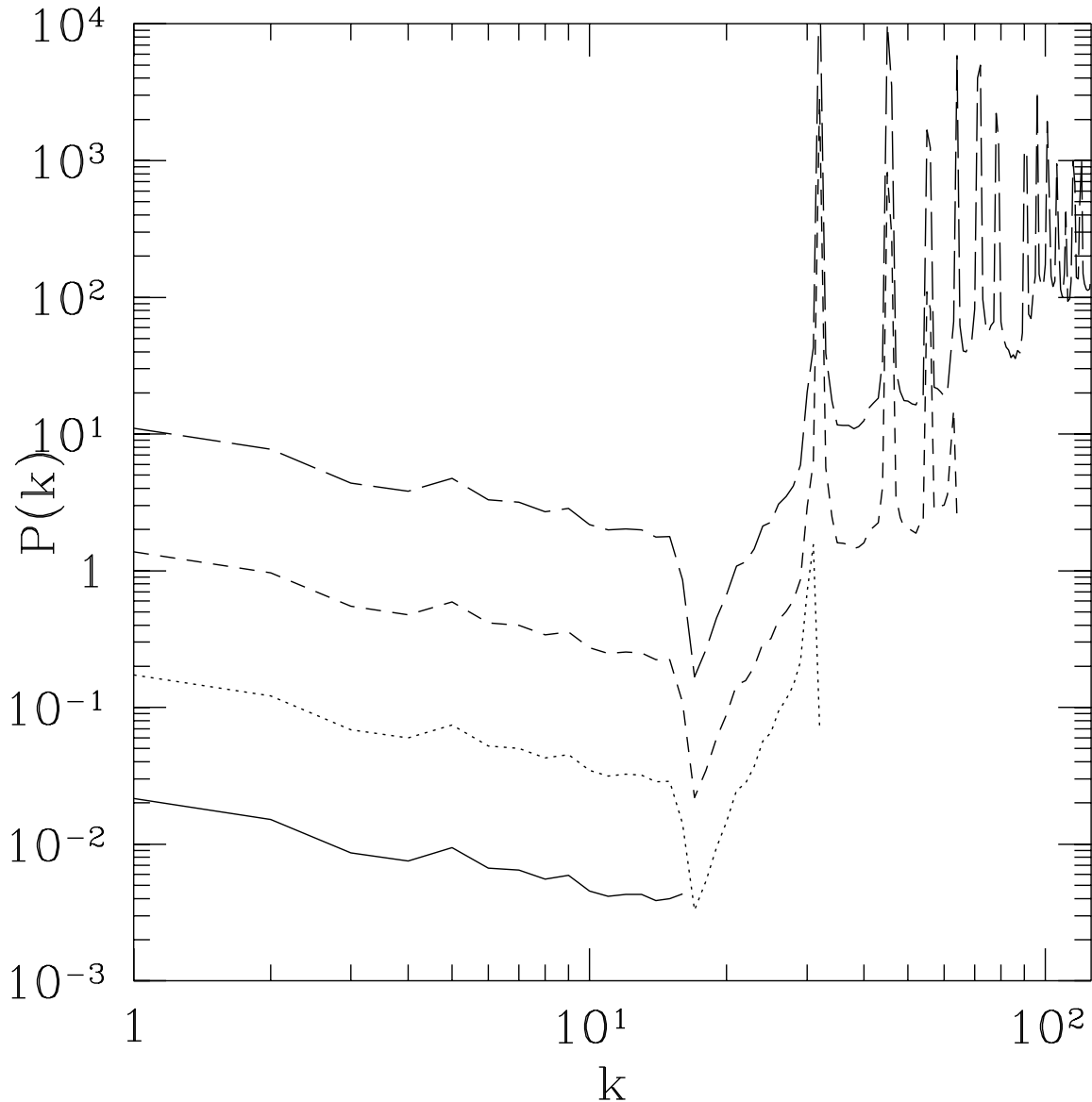


Fig. 5.— The power spectrum constructed using the  $32^3$  particles of the initial conditions for all except our  $k_c = 64k_f$  runs, as evaluated on mesh of size  $32^3$  (solid),  $64^3$  (dots),  $128^3$  (shortdash), and  $256^3$  (longdash), shown with vertical offset. The normalization is such that a Poisson distribution of points of the same number of particles as mesh cells on each mesh would converge to  $P(k) = 1$ . Normally, such spectra are only shown up to the particle Nyquist frequency, as in the solid line. The spikes are a result of the lattice of particles which is deformed to provide the initial conditions, and are of course not random phase. In HFLMR codes, this part of the initial conditions is evolved, with unknown consequences.

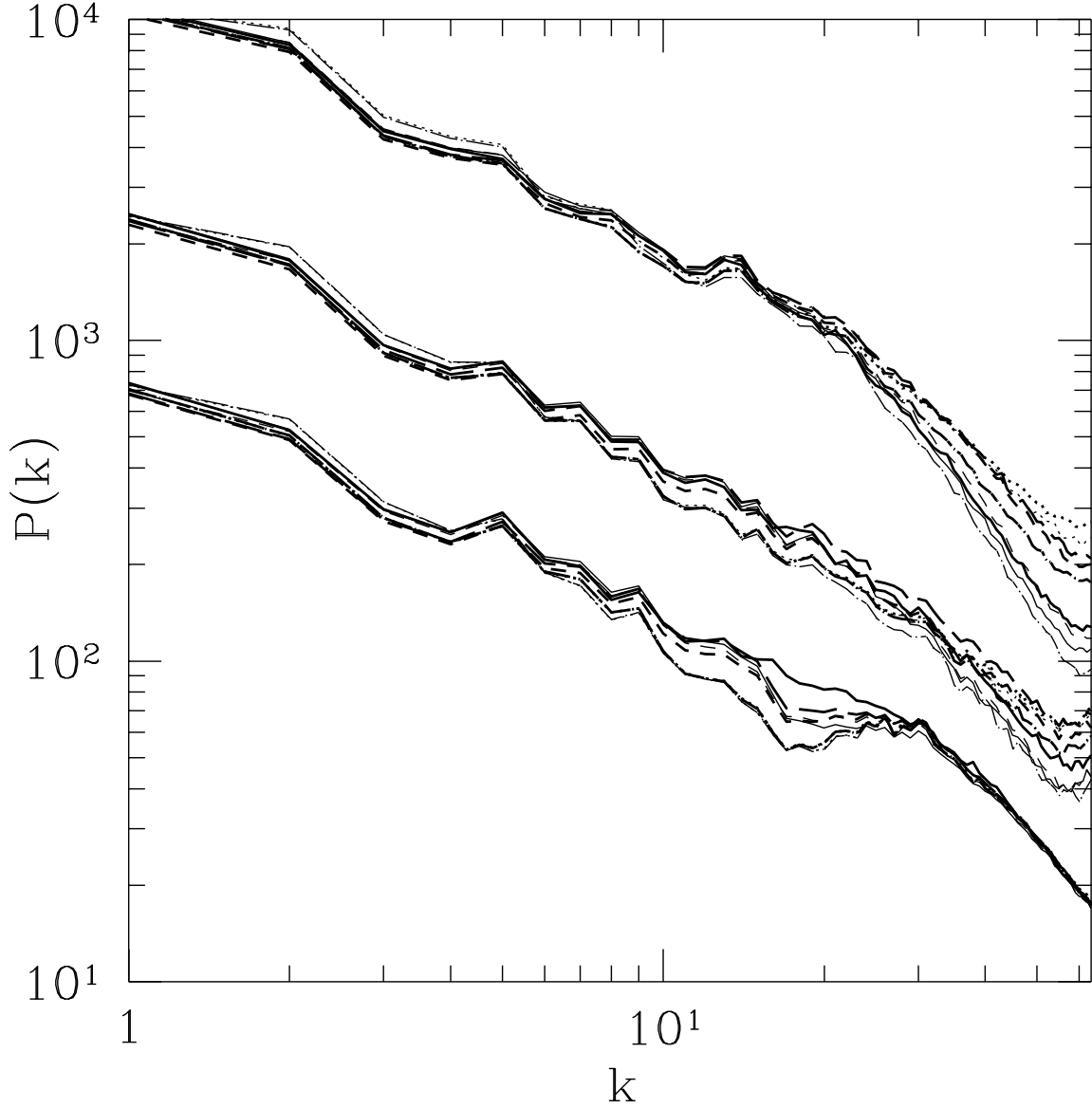


Fig. 6.— We show the power spectrum of the three successive evolved stages for all our simulations, evaluated from  $32^3$  particles on a  $128^3$  mesh their force resolution. The normalization is such that a Poisson distribution of  $128^3$  particles would converge to  $P = 1$ . The light solid line is the  $k_c = 16k_f$  PM run; the heavy solid line is the  $k_c = 64k_f$  PM run. Other heavy lines are P<sup>3</sup>M runs and light lines are tree code runs. Dotted lines:  $\epsilon = 0.0625$  runs with  $32^3$  particles. Longdash-dot:  $\epsilon = 0.25$  runs with  $32^3$  particles. Shortdash:  $\epsilon = 0.5$  runs with  $64^3$  particles. Longdash:  $\epsilon = 1.0$  run (P<sup>3</sup>M only) with  $128^3$  particles.

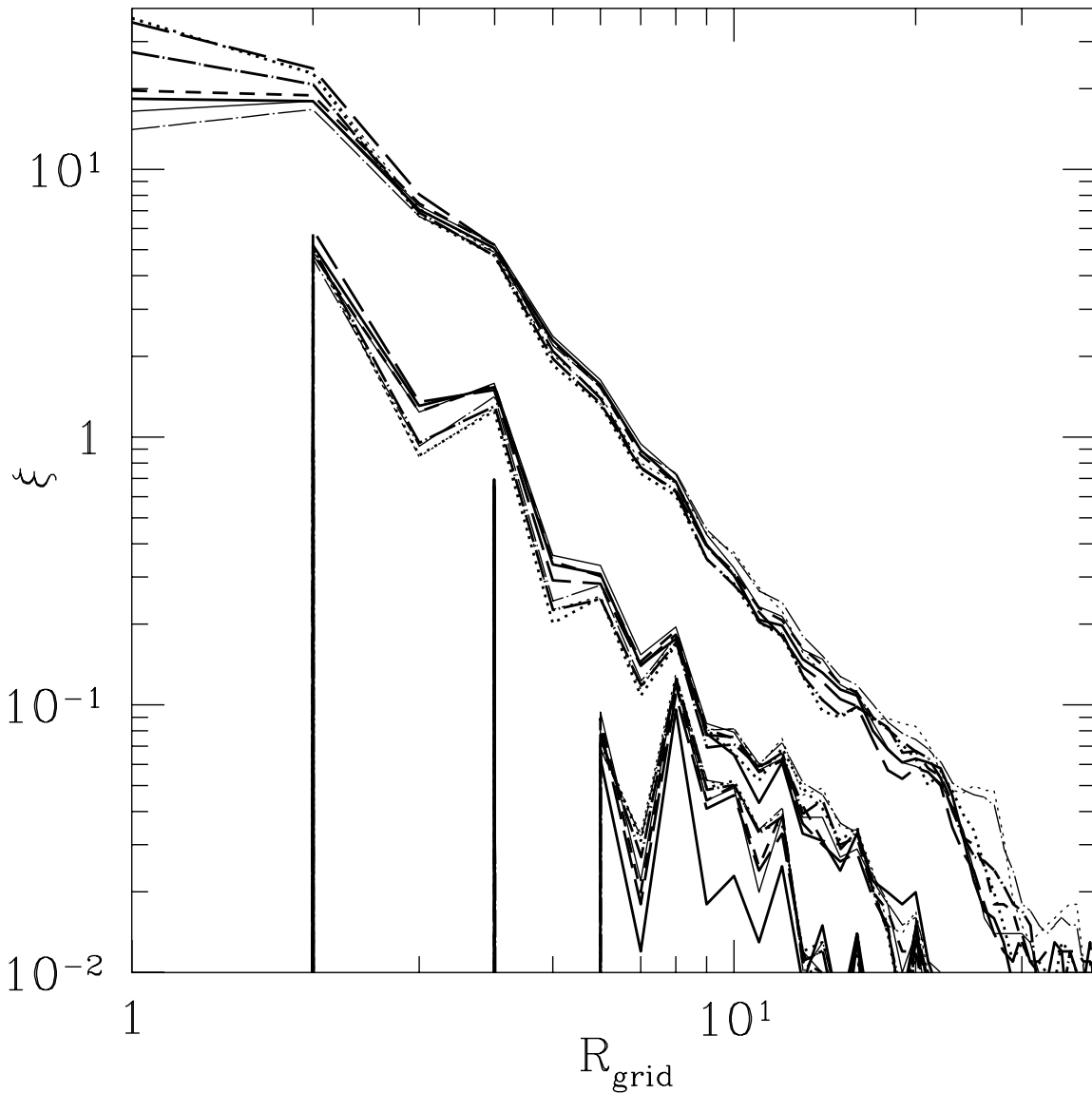


Fig. 7.— The two-point correlation function of all the mass in the simulations is shown for the same three stages shown in the power spectrum plot. Line types here and in all subsequent plots match Fig. 6. The spikes which exist at early stages are a relic of the lattice upon which the particles began, which is insufficiently deformed to be suppressed then. The last stage corresponds to nonlinearity sufficiently strong that boundary conditions would become a problem if the simulation were continued further.

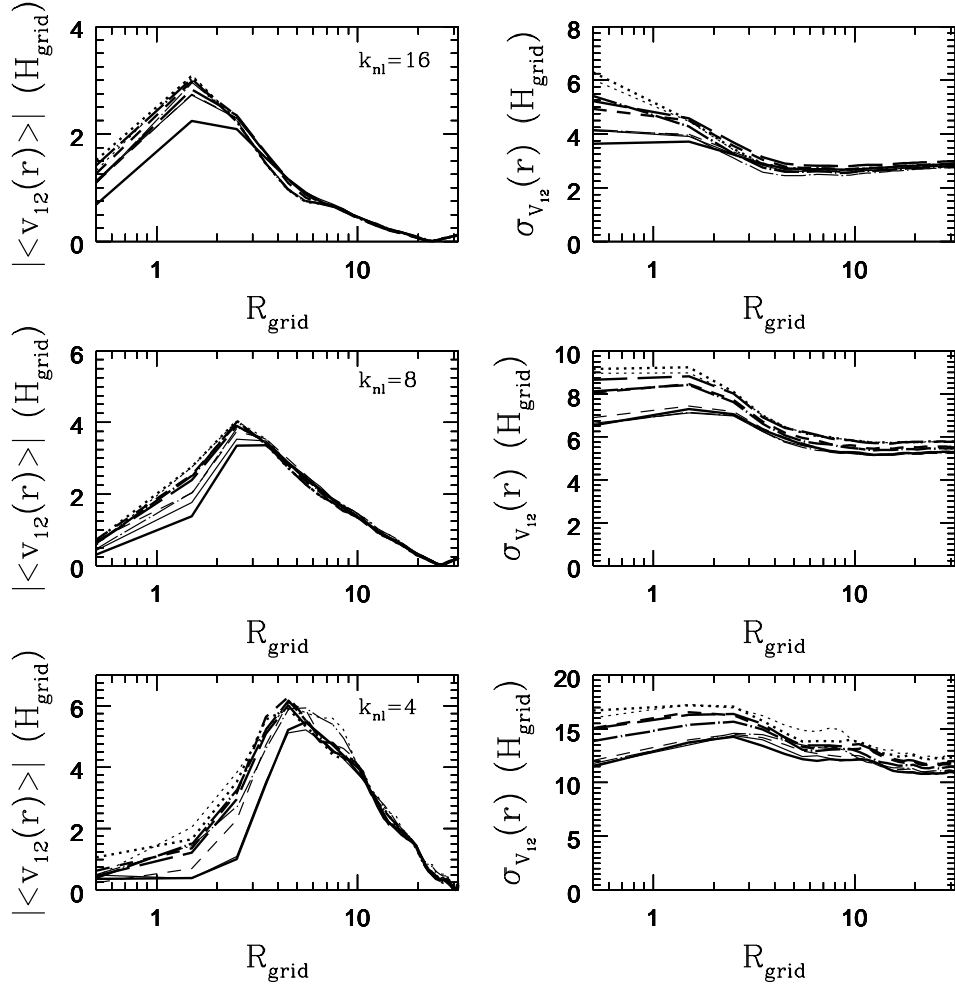


Fig. 8.— The pairwise velocity and pairwise dispersion, as defined in the text in Section 4.4 are plotted for each stage, using the usual line types. The force resolution scale is 1 for most of our runs, 0.25 for two. The mean interparticle separation of the sparsest runs is 4; convergence is not reached until approximately this scale (rather than the force resolution scale).

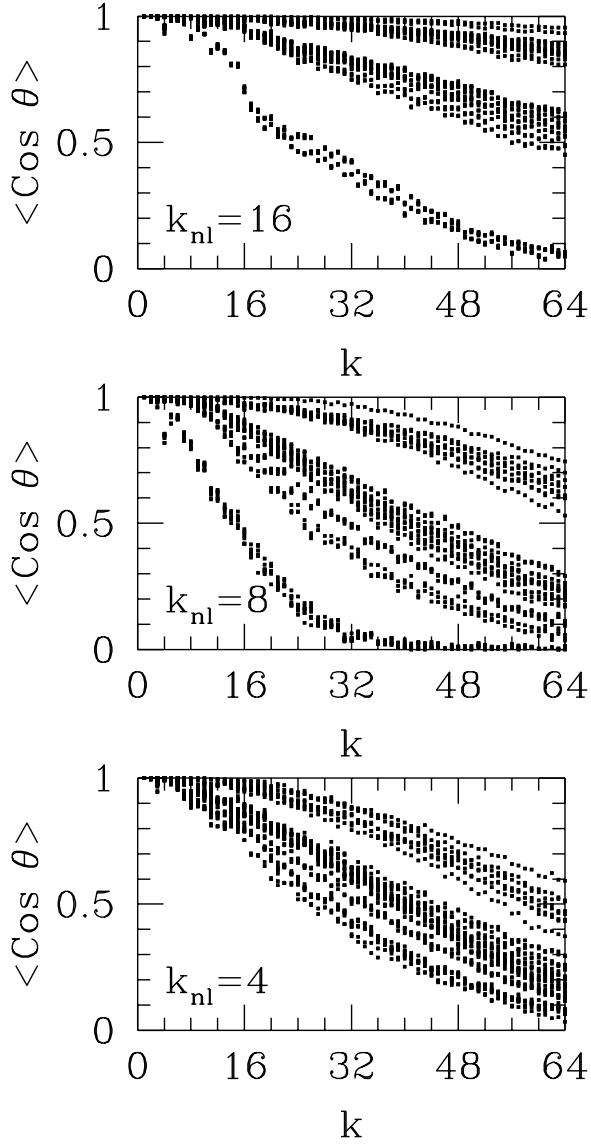


Fig. 9.— The successive plots contain all the data for the averaged phase agreement between *all* of the simulations runs at the same stage;  $\langle \text{cos}\theta \rangle$  is defined in the text and is 1 for agreement and 0 for uncorrelated phases. Individual functions are not distinguishable here, but it is clear that they fall into three classes, which are described in the text.

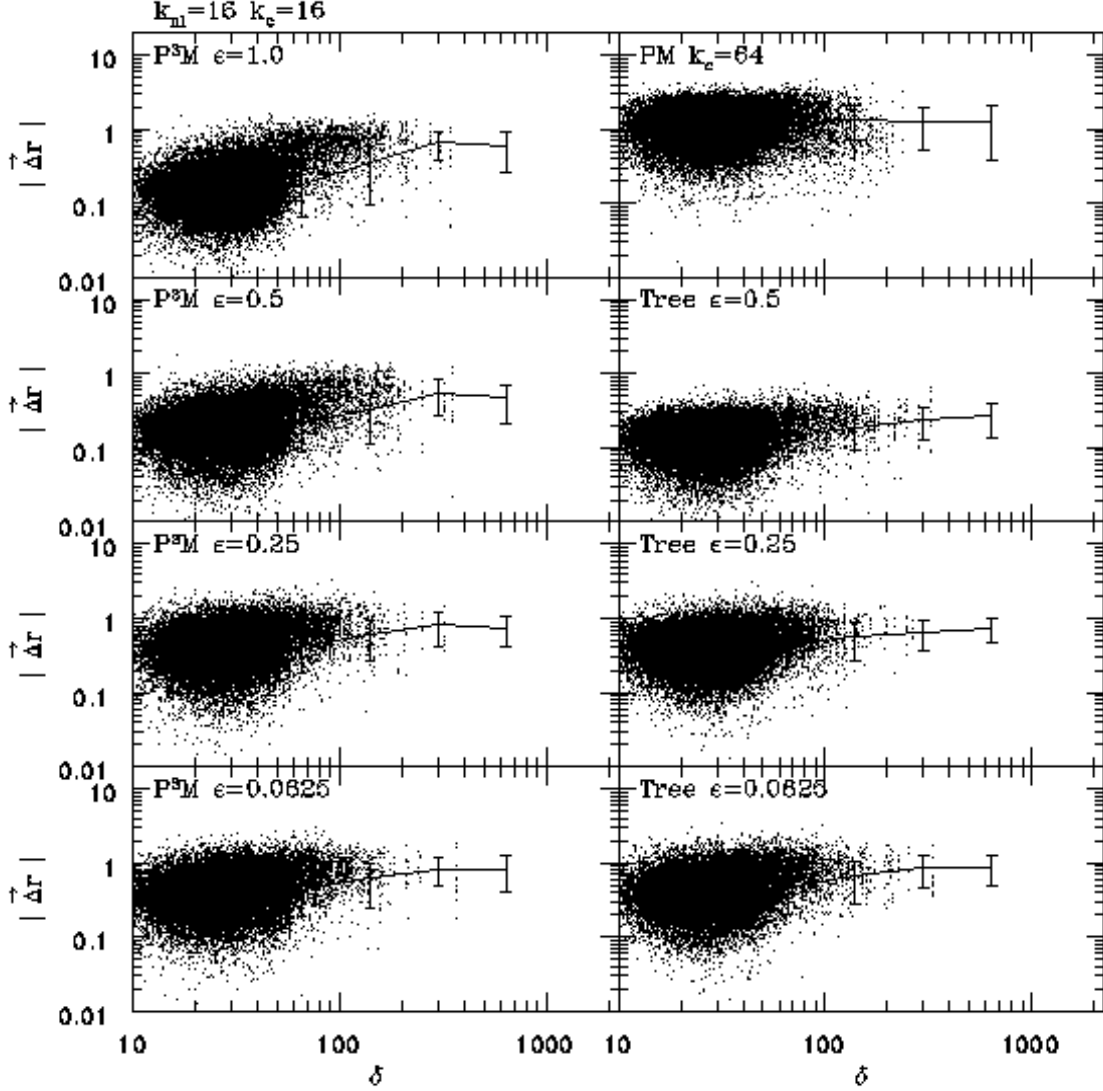


Fig. 10.— The scatter plots contain the difference in positions between particles which had the same initial position and velocity in the PM run with  $k_c = 16k_f$  and positions in other runs with identical initial conditions (and in the PM,  $k_c = 64k_f$  run, upper right); The distance is plotted against the local density of the simulation in the fiducial PM run. Shown here for the state  $k_{nl} = 16k_f$ .

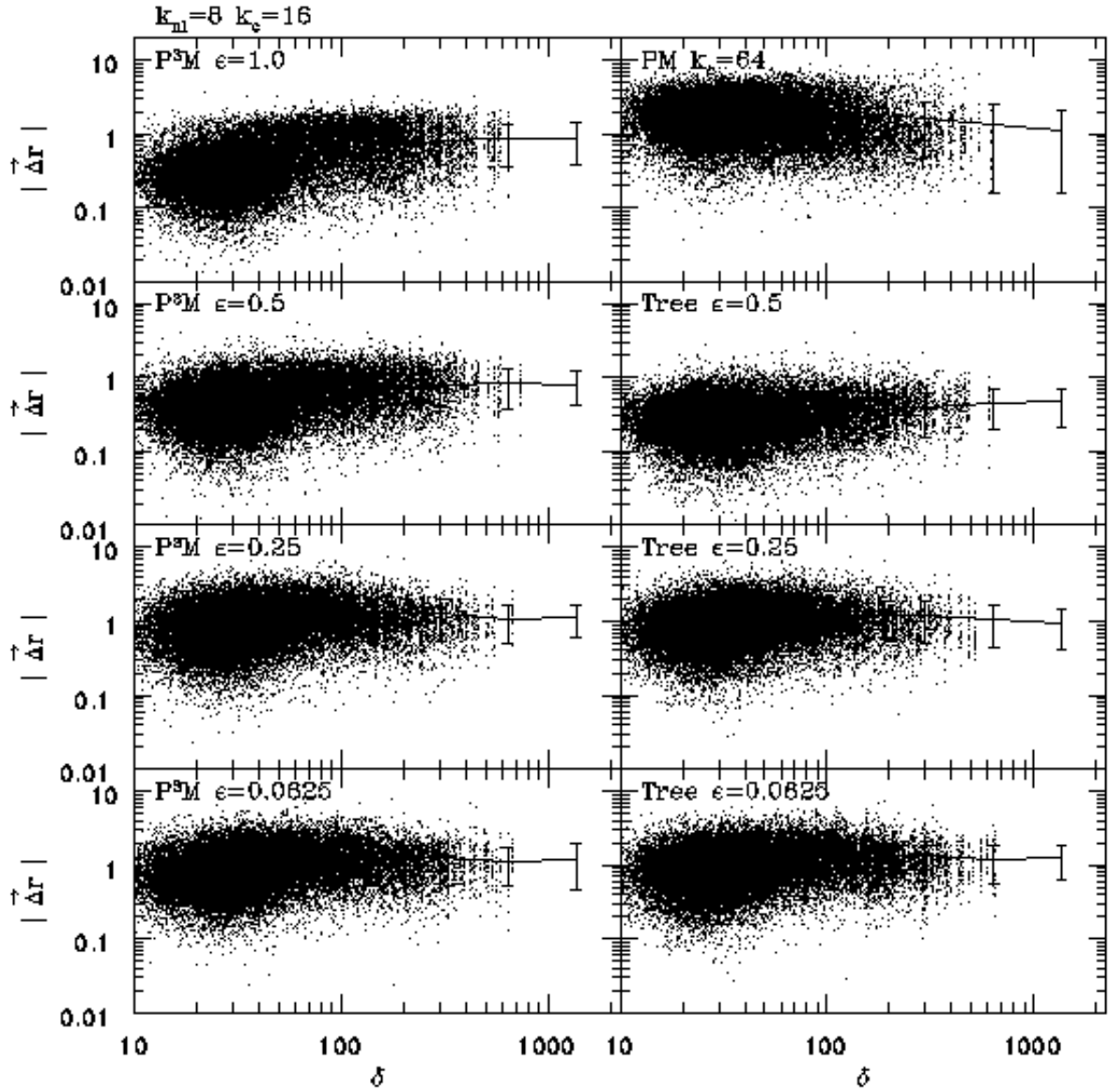


Fig. 11.— The same as Fig. 10, except for the state  $k_{nl} = 8k_f$ .

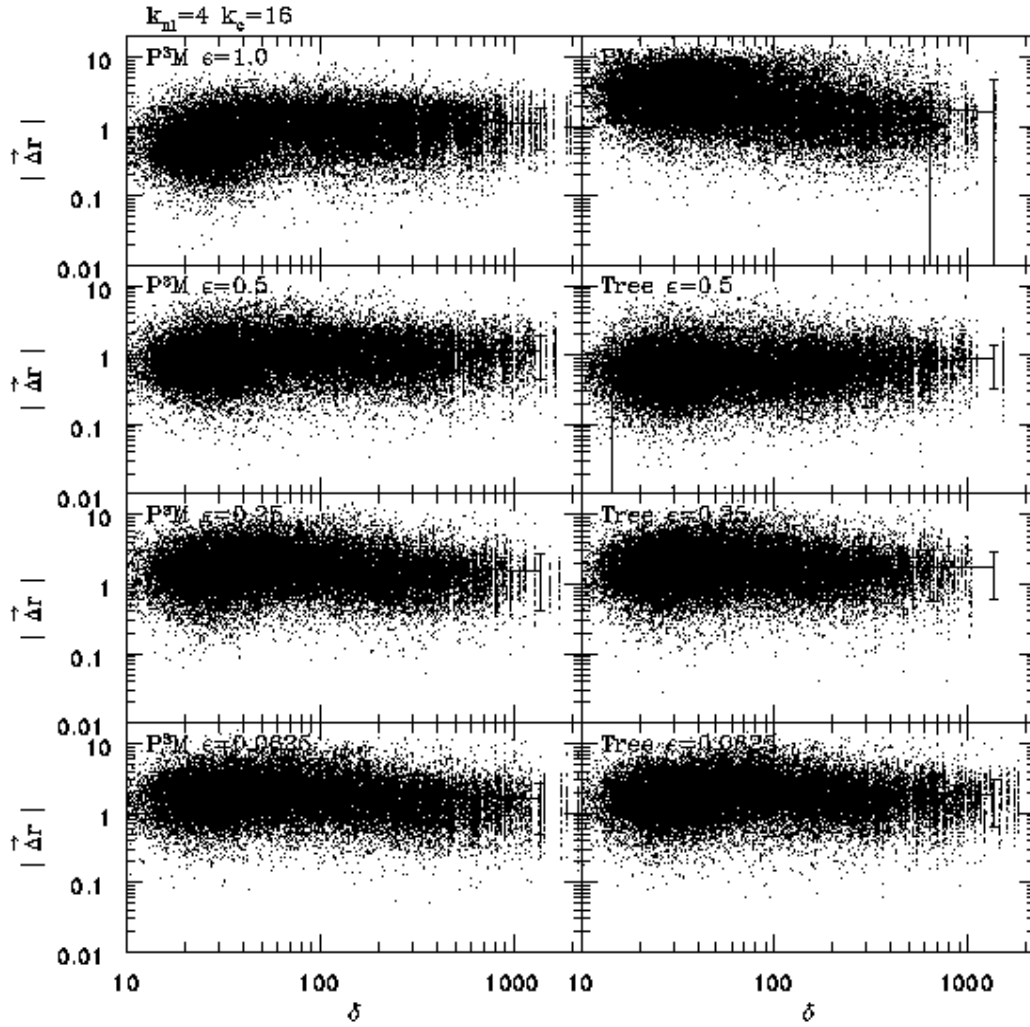


Fig. 12.— The same as Fig. 10, except for the state  $k_{nl} = 4k_f$ .

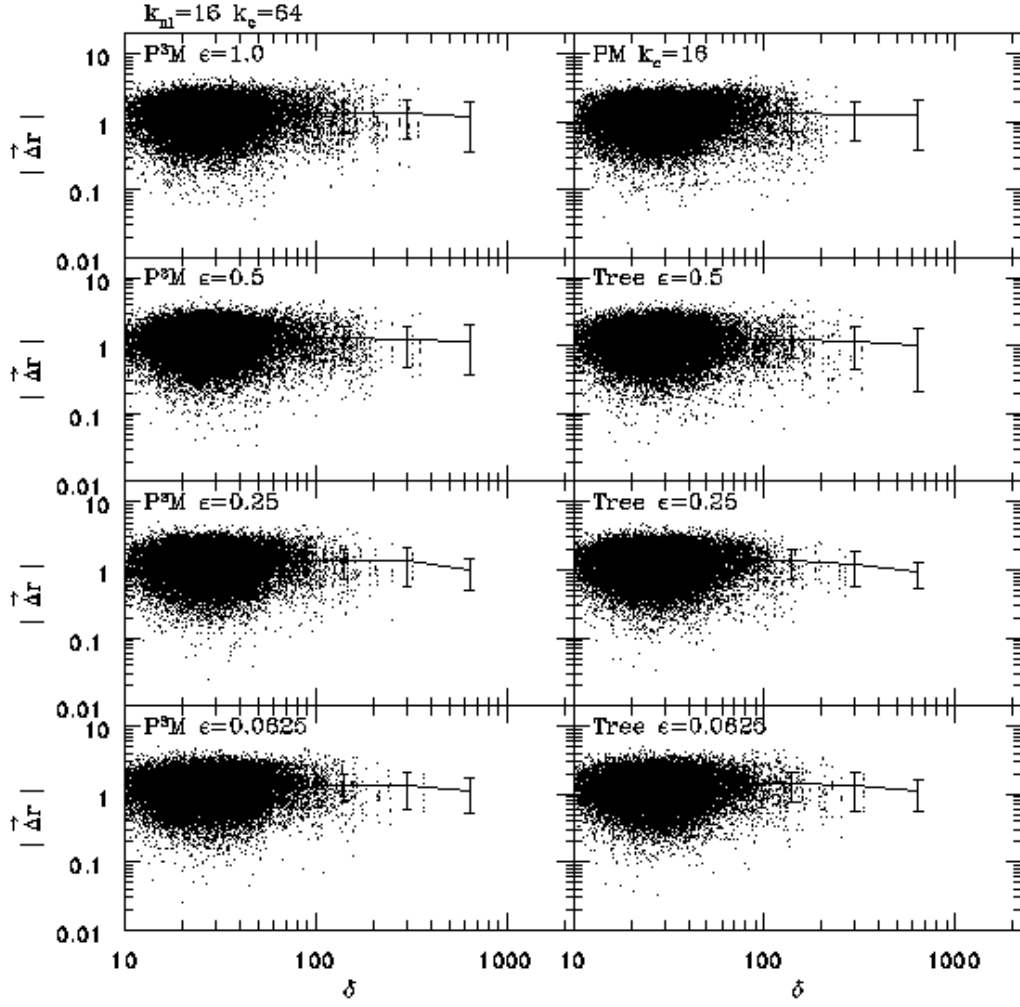


Fig. 13.— The same as Fig. 10, except that the displacements are from the positions of the particles in the  $k_c = 64k_f$  run, and the densities on the abscissa are drawn from that simulation. The stage shown here is  $k_{nl} = 16k_f$ .

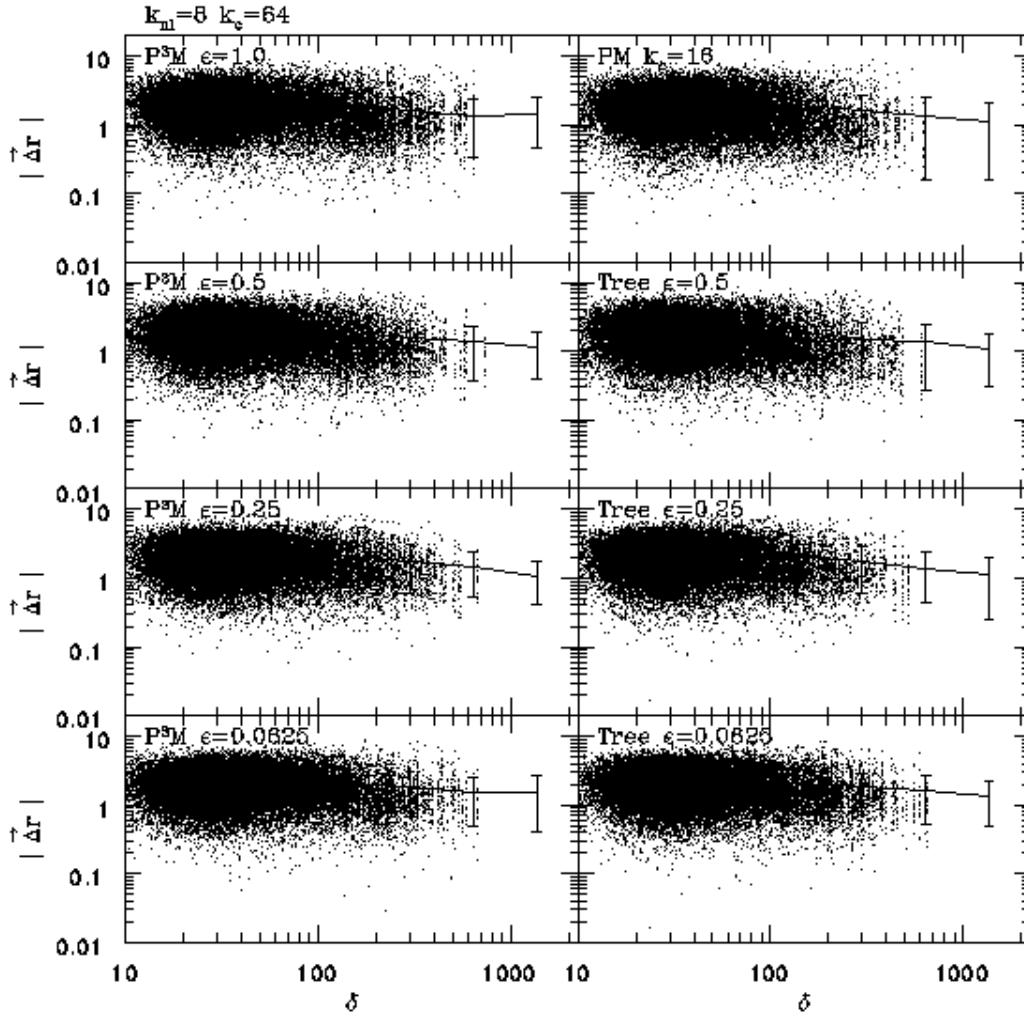


Fig. 14.— The same as Fig. 13, except for the state  $k_{nl} = 8k_f$ .

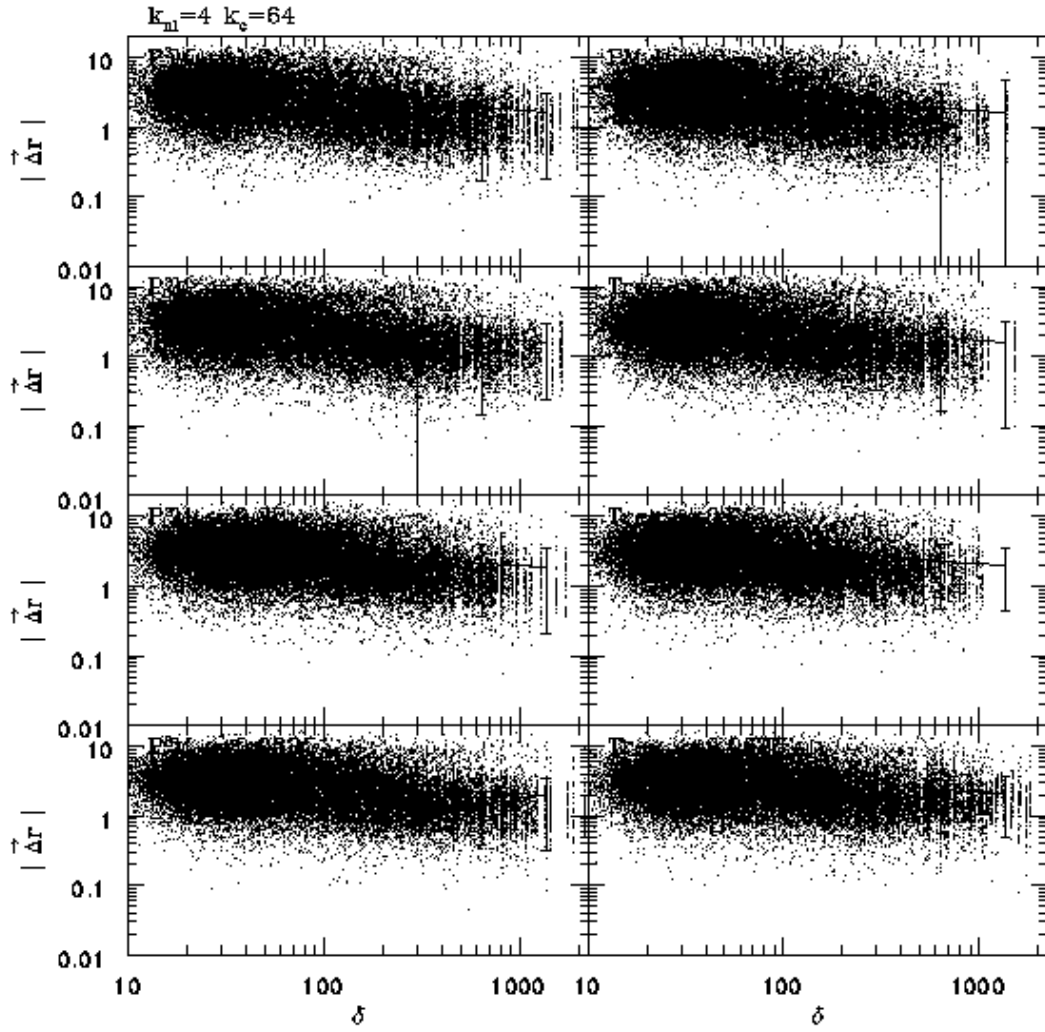


Fig. 15.— The same as Fig. 13, except for the state  $k_{nl} = 4k_f$ .

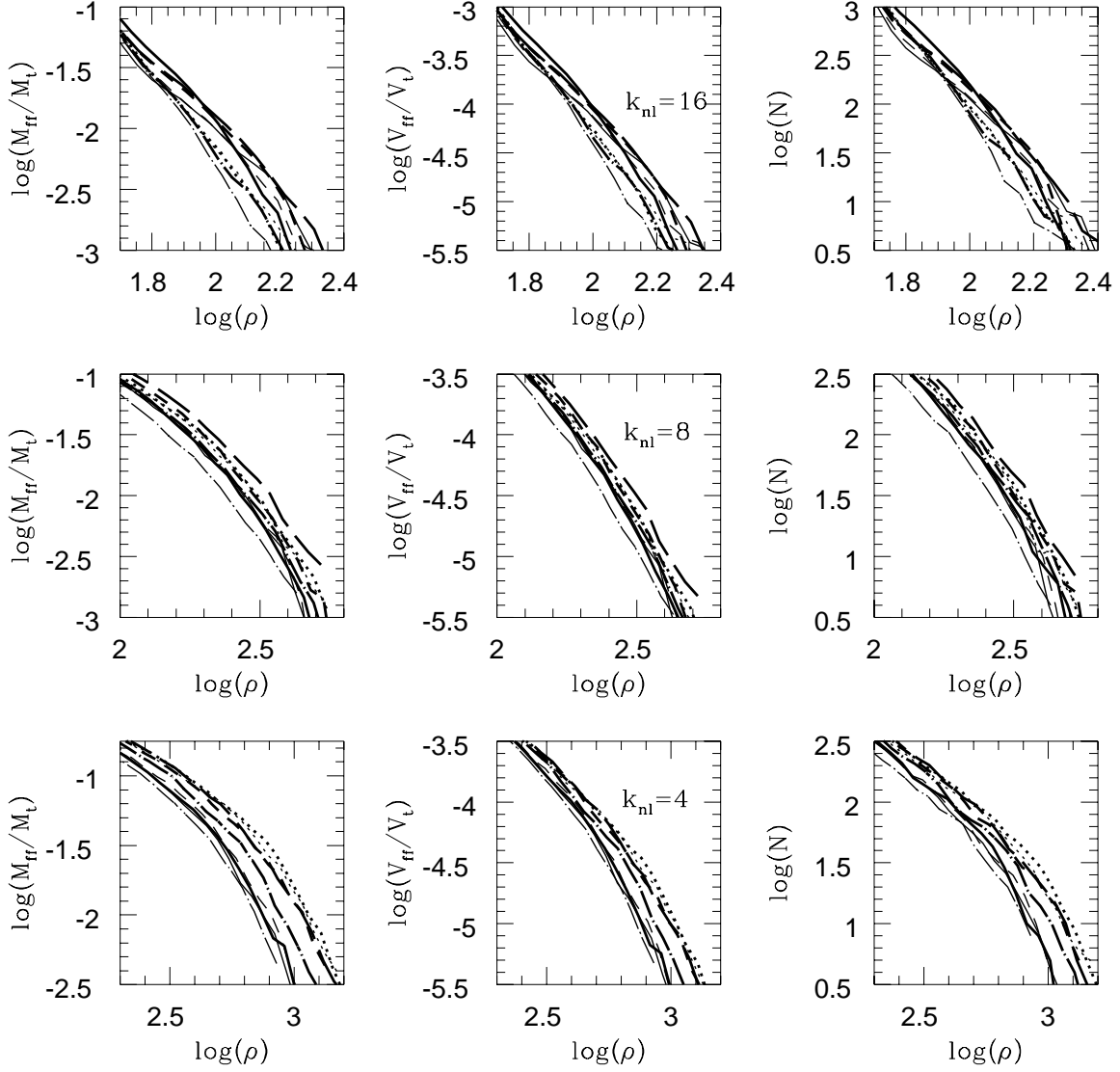


Fig. 16.— Three rows show three stages in the evolution of the models. The left column shows the fraction of mass, the middle column - the fraction of volume, and the right column - the number of disjoint regions having densities greater than the density threshold shown on the horizontal. The densities were calculated on the  $128^3$  mesh.

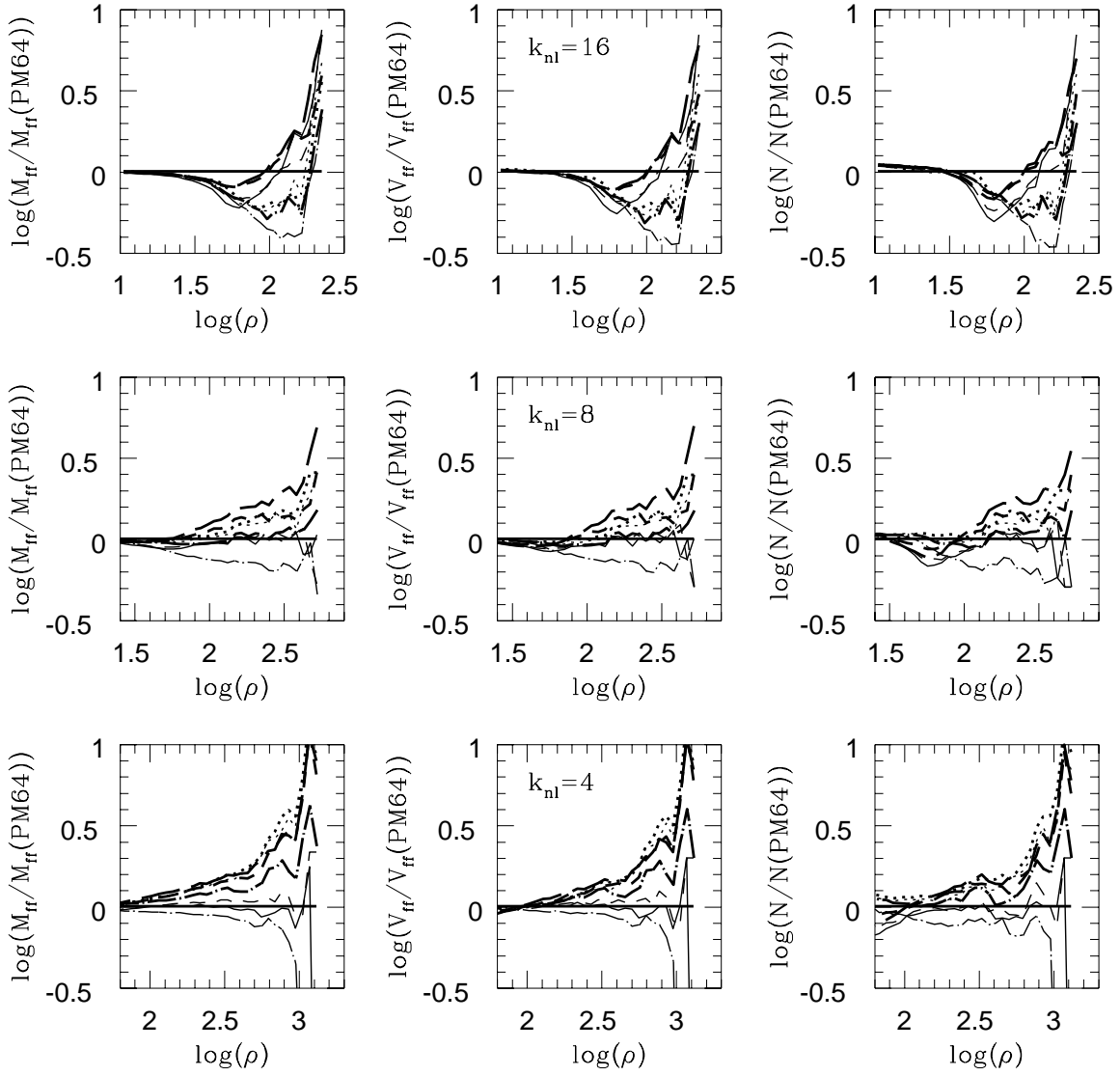


Fig. 17.— The ratios of the same parameters plotted in Fig. 16 to the fiducial PM model with  $N = 128^3$ , and  $k_c = 64$ .

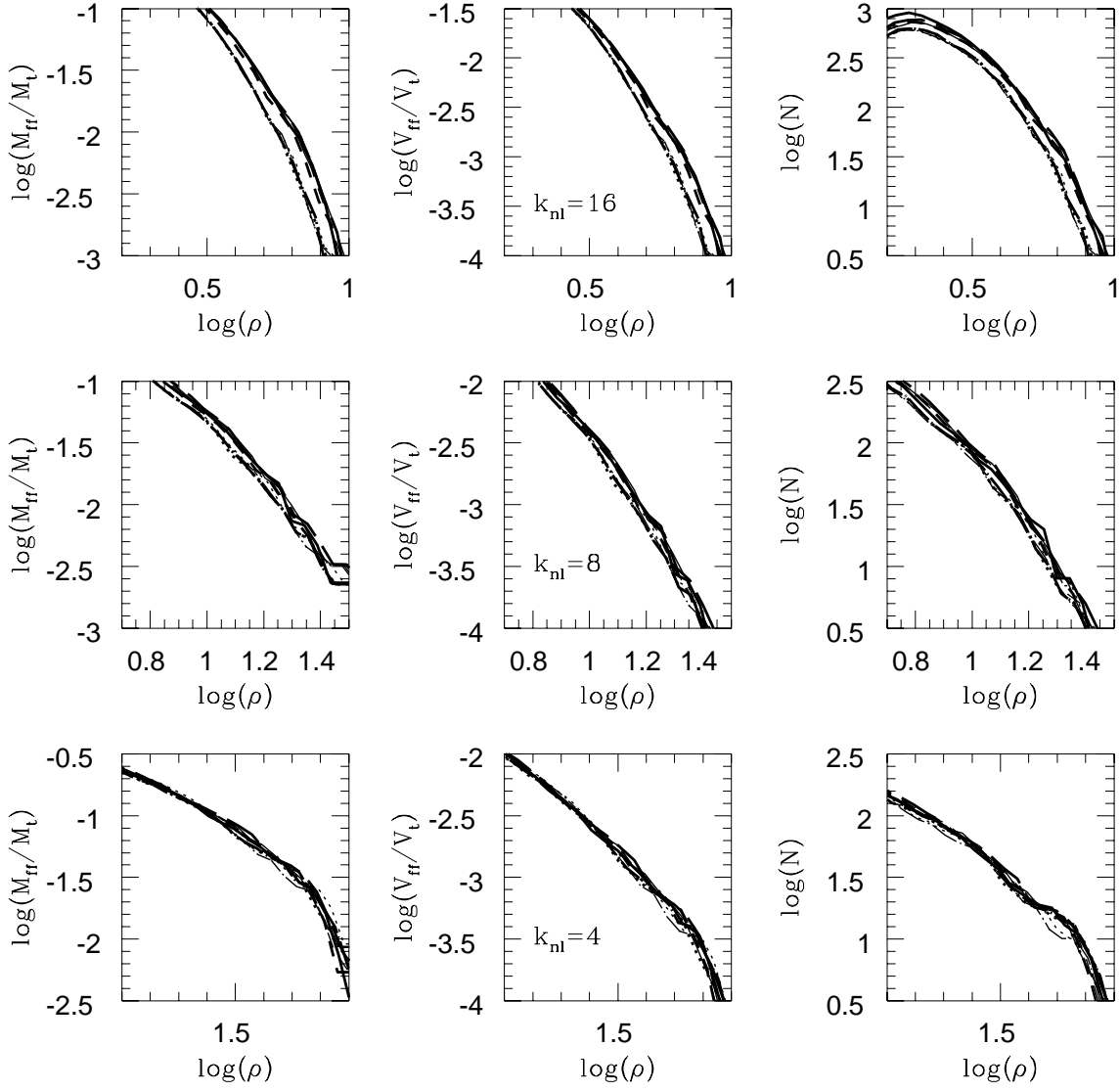


Fig. 18.— Same as Fig. 16 except the densities were calculated on  $32^3$  mesh.

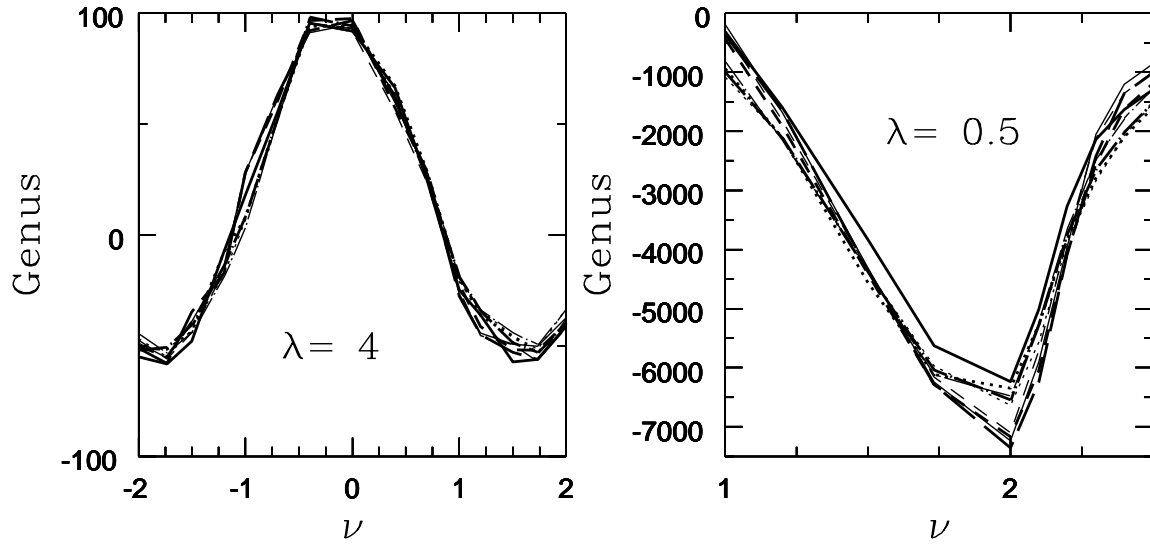


Fig. 19.— The genus is plotted for the final stage  $k_{nl} = 4$ : The left panel shows genus of the density fields smoothed on the scale of the mean particle separation; the right panel shows genus for the fields smoothed on half of the force resolution scale (only the part corresponding to high densities is shown).

Table 1. Model Parameters for the Test Cases

Code		N	$\bar{l}_{sep}$ <sup>a</sup>	$\epsilon_{force}$ <sup>b</sup>
PM	$k_c = 16$	$128^3$	1.0	1.0
	$k_c = 64$	$128^3$	1.0	1.0
P <sup>3</sup> M	$k_c = 16$	$32^3$	4.0	0.0625
	$k_c = 16$	$32^3$	4.0	0.25
	$k_c = 16$	$64^3$	2.0	0.5
	$k_c = 16$	$128^3$	1.0	1.0
Tree	$k_c = 16$	$32^3$	4.0	0.0625
	$k_c = 16$	$32^3$	4.0	0.25
	$k_c = 16$	$64^3$	2.0	0.5
	$k_c = 16$	$64^3$	2.0	0.5

<sup>a</sup> $\bar{l}_{sep}$  is the mean particle separation in grid cell units.

<sup>b</sup> $\epsilon_{force}$  is in units of the mean particle separation,  $\bar{l}_{sep}$ . Note that for most of the runs  $a \equiv \epsilon_{force} \times \bar{l}_{sep} = 1$ , only for two does  $a = 0.25$ .

Table 2. Cross-Correlations at  $k_{nl} = 16$

	PM		P <sup>3</sup> M				Tree		
	$k_c = 16$	$k_c = 64$	$128^3 \epsilon = 1.0$	$64^3 \epsilon = 0.5$	$\epsilon = 0.25$	$\epsilon = 0.0625$	$64^3 \epsilon = 0.5$	$\epsilon = 0.25$	$\epsilon = 0.0625$
PM ( $k_c = 16$ )	—	0.31	0.94	0.93	0.77	0.76	0.97	0.74	0.74
PM ( $k_c = 64$ )	0.92	—	0.31	0.30	0.26	0.26	0.31	0.26	0.26
P <sup>3</sup> M $128^3$ ( $\epsilon = 1.0$ )	1.00	0.91	—	0.95	0.72	0.72	0.95	0.69	0.69
P <sup>3</sup> M $64^3$ ( $\epsilon = 0.5$ )	1.00	0.91	1.00	—	0.81	0.81	0.97	0.78	0.77
P <sup>3</sup> M ( $\epsilon = 0.25$ )	0.99	0.91	0.98	0.99	—	0.98	0.81	0.96	0.96
P <sup>3</sup> M ( $\epsilon = 0.0625$ )	0.98	0.91	0.98	0.99	1.00	—	0.81	0.95	0.95
Tree $64^3$ ( $\epsilon = 0.5$ )	1.00	0.92	1.00	1.00	0.99	0.99	—	0.79	0.79
Tree ( $\epsilon = 0.25$ )	0.98	0.90	0.98	0.98	1.00	1.00	0.99	—	0.99
Tree ( $\epsilon = 0.0625$ )	0.98	0.90	0.98	0.98	1.00	1.00	0.99	1.00	—

Table 3. Cross-Correlations at  $k_{nl} = 8$

	PM		P <sup>3</sup> M				Tree		
	$k_c = 16$	$k_c = 64$	$128^3 \epsilon = 1.0$	$64^3 \epsilon = 0.5$	$\epsilon = 0.25$	$\epsilon = 0.0625$	$64^3 \epsilon = 0.5$	$\epsilon = 0.25$	$\epsilon = 0.0625$
PM ( $k_c = 16$ )	—	0.48	0.87	0.84	0.60	0.58	0.91	0.55	0.56
PM ( $k_c = 64$ )	0.94	—	0.47	0.46	0.40	0.40	0.46	0.37	0.38
P <sup>3</sup> M $128^3$ ( $\epsilon = 1.0$ )	1.00	0.94	—	0.88	0.59	0.57	0.86	0.53	0.54
P <sup>3</sup> M $64^3$ ( $\epsilon = 0.5$ )	1.00	0.94	1.00	—	0.65	0.63	0.90	0.58	0.59
P <sup>3</sup> M ( $\epsilon = 0.25$ )	0.97	0.92	0.97	0.98	—	0.92	0.64	0.86	0.87
P <sup>3</sup> M ( $\epsilon = 0.0625$ )	0.96	0.92	0.97	0.97	1.00	—	0.62	0.83	0.84
Tree $64^3$ ( $\epsilon = 0.5$ )	1.00	0.94	0.99	1.00	0.98	0.98	—	0.61	0.61
Tree ( $\epsilon = 0.25$ )	0.96	0.92	0.96	0.96	0.99	0.99	0.97	—	0.93
Tree ( $\epsilon = 0.0625$ )	0.96	0.92	0.96	0.96	0.99	0.99	0.97	1.00	—

Table 4. Cross-Correlations at  $k_{nl} = 4$

	PM		P <sup>3</sup> M				Tree		
	$k_c = 16$	$k_c = 64$	$128^3 \epsilon = 1.0$	$64^3 \epsilon = 0.5$	$\epsilon = 0.25$	$\epsilon = 0.0625$	$64^3 \epsilon = 0.5$	$\epsilon = 0.25$	$\epsilon = 0.0625$
PM ( $k_c = 16$ )	—	0.65	0.83	0.80	0.64	0.61	0.84	0.52	0.49
PM ( $k_c = 64$ )	0.96	—	0.63	0.63	0.57	0.55	0.63	0.47	0.44
P <sup>3</sup> M $128^3$ ( $\epsilon = 1.0$ )	0.99	0.95	—	0.89	0.66	0.64	0.84	0.50	0.48
P <sup>3</sup> M $64^3$ ( $\epsilon = 0.5$ )	0.99	0.96	0.99	—	0.68	0.66	0.84	0.49	0.47
P <sup>3</sup> M ( $\epsilon = 0.25$ )	0.96	0.94	0.97	0.97	—	0.86	0.67	0.70	0.67
P <sup>3</sup> M ( $\epsilon = 0.0625$ )	0.96	0.94	1.00	1.00	1.00	—	0.63	0.63	0.63
Tree $64^3$ ( $\epsilon = 0.5$ )	1.00	0.96	0.99	0.99	0.97	0.97	—	0.60	0.56
Tree ( $\epsilon = 0.25$ )	0.92	0.90	0.92	0.92	0.96	0.96	0.94	—	0.87
Tree ( $\epsilon = 0.0625$ )	0.92	0.90	0.91	0.91	0.96	0.96	0.94	1.00	—